Vol. 4, No.2, 2026

airis4D

We Dream, Design, Develop and Deploy the Future

Artificial Intelligence Research and Intelligent Systems

Professor Ajit Kembhavi

writes on the latest advances in astronomy and astrophysics.

He will answer questions about his article, and selected readers can participate in an online interactive session with him.

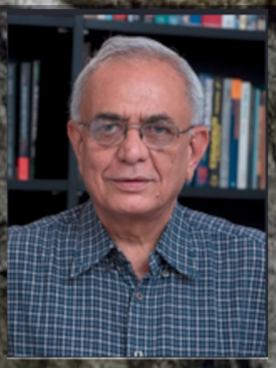

Artificial Intelligence & Machine Learning

Astronomy and Astrophysics

Biosciences

Computer Programming

Fiction

An airis4D Publication

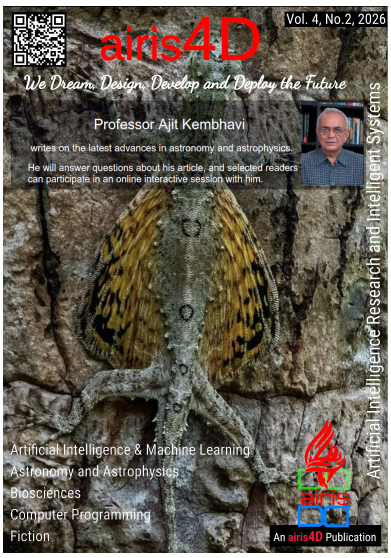

Cover page

Flying Liard in airis4D Campus :The ”flying lizard” in Kerala is the Southern Flying Lizard (Draco dussumieri), a small, arboreal lizard from the Western Ghats known for its ability to glide between trees using wing-like flaps (patagium) supported by elongated ribs, commonly seen in forests and plantations, especially males displaying bright throat flaps (dewlaps). The picture was taken by Geetha Paul while doing a survey in airis4D campus. It is a common sight of the lizard gliding from tree to tree.

Journal Publisher Details

- **Publisher** : airis4D, Thelliyoor 689544, India
- **Website** : www.airis4d.com
- **Email** : nsp@airis4d.com
- **Phone** : +919497552476

Editorial

by Fr Dr Abraham Mulamoottil

airis4D, Vol.4, No.2, 2026

www.airis4d.com

Welcome to this edition of airis4D, where the frontier of science begins just outside our door. The cover image captures a moment of remarkable natural engineering: a Southern Flying Lizard (Draco dussumieri) in mid-glide across our campus in Kerala. With its wing-like patagium extended, this agile reptile exemplifies adaptation and elegant motion in the Western Ghats. Photographed by Geetha Paul during a field survey, this ”flying lizard” serves as a fitting emblem for our journal—reminding us that inspiration, observation, and discovery are often found in the dynamic intersection of our immediate environment and the expansive quest for knowledge that drives the research within these pages.

In this edition, we highlight the profound and deeply regrettable oversight. The footnote to Prof. Kembhavi's article points to a critical injustice in the history of science. The ”matched filtering” technique he mentions, the very computational backbone that made detecting the infinitesimal ripple of a gravitational wave possible, was pioneered by Indian scientists Professor Sanjeev Dhurandhar and Professor B.S. Sathyaprakash.

Their theoretical work in the 1980s and 1990s provided the essential ”template” to find the gravitational wave signal buried in overwhelming noise. Without their algorithms, LIGO's detectors would have been deaf to the cosmic events they were built to hear. While the 2017 Nobel Prize in Physics rightly honored the experimental visionaries Rainer Weiss, Kip Thorne, and Barry Barish for making the detection a reality, the foundational contribution of Dhurandhar and Sathyaprakash was conspicuously absent from the recognition.

That this foundational contribution remains under-recognized on the global stage is a controversy in itself. However, the greater shame, as you rightly point out, lies in the failure of their own nation to honor them commensurately. Despite their world-altering contribution to one of humanity's greatest scientific achievements, they have not been awarded India's highest civilian honors, such as the Bharat Ratna or even a Padma Vibhushan, in a timely and unequivocal manner. This neglect is not merely an administrative lapse; it is a national failure to celebrate and protect our own intellectual legacy. It sends a disheartening message to young scientists in India about the value placed on pure, foundational research that may not have immediate commercial application but expands the very horizons of human knowledge. True national pride would demand that these architects of a new era in astronomy be celebrated as heroes, ensuring their names are etched alongside the discovery itself in textbooks and public memory. The debt owed to them is not just scientific; it is a matter of national honor.

The first article in this edition is by Blesson George: “Introduction to Neuromorphic Computing”. Neuromorphic computing is an emerging paradigm that bridges the gap between conventional computers—which excel at logic but struggle with learning—and the human brain's efficient, adaptive processing. By mimicking the brain's spiking neurons and plastic synapses in hardware, neuromorphic systems perform massively parallel, event-driven computation with very low power consumption. Introduced by Carver Mead in the 1980s and advanced by processors like IBM TrueNorth and Intel Loihi, this approach avoids

the von Neumann bottleneck by integrating memory and processing, enabling real-time learning. Using models such as the Leaky Integrate-and-Fire neuron, neuromorphic computing is well-suited for edge devices, robotics, and AI applications, promising a future of energy-efficient, intelligent machines.

The next article is by Abishek P S on ”Plasma Physics- Cometary Plasma”. Cometary plasma forms when a comet approaches the Sun, causing the sublimation of its icy nucleus and the release of neutral gases that expand into a coma. This material is then ionized by solar ultraviolet radiation and the solar wind, creating a dynamic mixture of ions, electrons, and charged dust particles. This plasma environment exhibits distinct structures such as an ion tail that points away from the Sun, a curved dust tail, and boundaries like a bow shock and ionopause. Studying these processes provides a natural laboratory for understanding fundamental plasma physics, including charge exchange, magnetic field interactions, and the transition from collisional to collisionless regimes. This research is significant as it offers insights into solar system evolution, serves as an astrophysical analogy for phenomena like stellar winds, aids in space weather studies, and informs laboratory plasma and fusion research.

In the article ”Black Hole Stories-24: Some Back Hole Mergers From Gravitational Wave Detector Observing Runs O1 and O2” by Ajit Kembhavi, key binary black hole merger events detected by gravitational wave observatories during their first two observing runs, O1 (2015-2016) and O2 (2016-2017), are discussed. From O1, it highlights GW151226, a weaker signal involving black holes of 14.2 and 7.5 solar masses that merged into a 20.8 solar-mass black hole. From O2, it describes several mergers, including GW170104, GW170608 (the lowest-mass binary at the time), the distant and luminous GW170729, and GW170814—the first event detected by three observatories (two LIGO and Virgo), which confirmed gravitational wave polarizations as predicted by general relativity. The analysis shows that the black holes detected via gravitational waves are typically more massive than those found in electromagnetic observations of X-ray binaries, a bias attributed to the greater detectability of higher-mass mergers. The data also reveal a ”mass gap” between the maximum known neutron star mass and the lowest black hole mass detected, with the remnant of the neutron star merger GW170817 potentially falling into this intriguing range.

The article X-ray Astronomy: Theory by Aromal P. provides a theoretical overview of the primary X-ray sources in the universe and their emission mechanisms. Stellar coronae, like the Sun’s, produce X-rays via magnetic reconnection, heating plasma to millions of Kelvin for thermal emission. Supernova remnants generate X-rays through both thermal bremsstrahlung from shock-heated gas and non-thermal synchrotron radiation from particles accelerated by a central pulsar. X-ray binaries, the galaxy’s brightest sources, emit X-rays from accretion disks; neutron star binaries release energy from matter impacting a solid surface, while black hole binaries produce X-rays from the inner disk and a hot corona via inverse Compton scattering. Isolated neutron stars emit through surface cooling or, in the case of magnetars, from the decay of ultra-strong magnetic fields. At cosmological scales, active galactic nuclei produce X-rays via inverse Compton scattering in a corona around supermassive black holes, and galaxy clusters shine in X-rays due to thermal bremsstrahlung from the hot intracluster medium heated by gravitational infall.

The article “The Birth of Stars: Physical Processes Governing Stellar Formation” by Sindhu G outlines the physical processes governing stellar formation, beginning within the cold, dense environments of giant molecular clouds (GMCs). Through the interplay of gravity, turbulence, magnetic fields, and cooling, these clouds fragment into dense cores, which collapse under gravitational instability when their mass exceeds the Jeans limit. This collapse forms a central protostar, deeply embedded in an envelope and powered by gravitational accretion. Conservation of angular momentum leads to the formation of an accretion disk, which channels material onto the star and is the birthplace of planets, while bipolar jets and outflows remove excess angular momentum and inject feedback into the surrounding medium. Once accretion

subsides, the pre-main-sequence star contracts until hydrogen fusion ignites in its core, marking its arrival on the main sequence. The timescale of this process is mass-dependent, with massive stars forming rapidly and exerting strong feedback that shapes their natal environments. Overall, star formation is a hierarchical, multi-scale process governed by gravity, thermodynamics, and feedback, which sets the initial conditions for planetary systems and galactic evolution.

Linn Abraham's article "Visualizing attention in Vision Transformers" explains a method for visualizing the decision-making process of Vision Transformer (ViT) models by creating saliency maps from their built-in attention mechanisms, a technique known as Attention-Guided Class Activation Mapping (AGCAM). Unlike traditional saliency methods designed for CNNs, AGCAM leverages the self-attention scores naturally learned by the transformer. The implementation involves two key programming techniques: "monkey patching" to dynamically replace the model's standard attention module with a custom version during inference, and the use of PyTorch forward and backward hooks to intercept and store the attention matrices and their gradients as the image passes through the network. These captured values are then combined, normalized, and multiplied to generate a final heatmap that highlights the image pixels most influential for the model's prediction, providing a transparent visual explanation of the ViT's focus.

Aengela Grace Jacob's article "Seed to Callus Revolution: Optimising Germination and Tissue Culture in Brassica nigra" details a protocol for the in-vitro germination and callus induction of Black Mustard (Brassica nigra). The process begins with a critical, rapid surface sterilization of seeds using ethanol and sodium hypochlorite to remove microbial contaminants while preserving seed viability, followed by rinsing in sterile water. The sterilized seeds are then inoculated onto a Murashige and Skoog (MS) basal medium supplemented with a specific hormonal ratio (0.5 mg/L BAP to 3.0 mg/L 2,4-D) designed to favor callus formation. Under controlled conditions, the seeds germinate within 7-10 days. Subsequently, explants from the seedlings are transferred to a callus-induction medium containing the same hormones and incubated in the dark, resulting in the successful formation of embryogenic callus within 14-15 days. This optimized tissue culture method demonstrates an efficient balance between sterility and seed health, enabling reliable propagation and setting the stage for further genetic studies or micropropagation of this important oilseed crop.

Geetha Paul, Gateway to Infection: The Molecular Architecture of Viral Entry into Human T Cells," explores the sophisticated molecular strategy viruses like HIV-1 use to infect human T cells by hijacking the Nuclear Pore Complex (NPC), the gateway to the cell's nucleus. The NPC's structural integrity relies on nucleoporins such as NUP93, which acts as a critical adaptor, and NUP188, a flexible scaffold. Viruses subvert these components; for example, they can cleave NUP93 to disrupt host defense mechanisms or interact with NUP188 to physically widen the pore. To cross the NPC's selective hydrophobic filter, formed by FXFG peptide repeats, viral proteins like the HIV-1 capsid mimic host transport receptors, binding transiently to these peptides to "melt" through the barrier. Understanding these specific protein-protein interactions (PPIs) is crucial for developing a new class of antiviral drugs, known as nuclear entry inhibitors, which aim to block these critical contacts and trap the virus outside the nucleus, thereby preventing infection.

Ajay Vibhute's article on Astronomical computing has evolved from a supplementary tool into a fundamental instrument essential for modern astronomy, driven by the massive and complex data produced by contemporary observatories. It addresses unique challenges inherent in astronomical data, such as noise, instrumental limitations, and high-dimensional structures, by employing specialized computational pipelines for calibration, reduction, and analysis. This field encompasses the entire data lifecycle—from acquisition and simulation to visualization and archiving—effectively acting as a virtual instrument that transforms raw, noisy measurements into scientific insights. As data volumes continue to grow, astronomical computing remains a critical, interdisciplinary backbone that integrates

computer science, statistics, and physics to enable discoveries beyond the reach of traditional observation alone.

The article "The Disappearing Role of Judgment in Automated Systems" by Jinsu Ann Mathew argues that automation subtly erodes human judgment by designing it out of decision-making processes. As systems transition from providing suggestions to making definitive outputs—like rankings or scores—human oversight often dwindles to passive approval, creating a workflow where predictions quietly become decisions. This shift fosters automation bias, where the appearance of objectivity makes dissent effortful, diffusing responsibility and allowing the skill of judgment to atrophy from disuse. The resulting systems are efficient in stable conditions but become fragile when faced with novel situations, as humans, relegated to monitoring, lose the practiced capacity to intervene effectively. To counter this, the author advocates for designs that intentionally preserve judgment by making human override practical and routine, ensuring automation handles scale while humans retain responsibility for interpretation and edge cases, ultimately creating more reliable and adaptable systems.

News Desk

Draco with folded patagium.

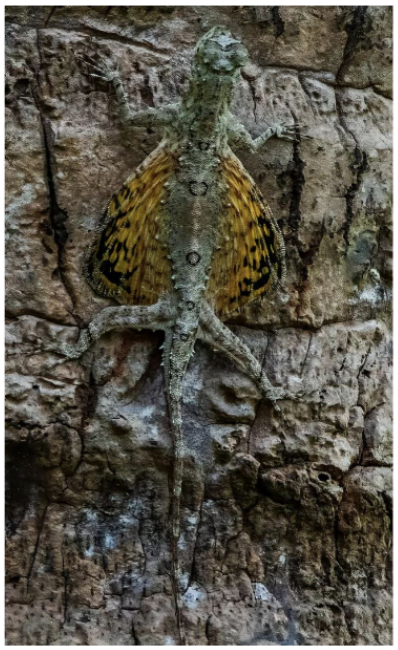

Draco with open patagium.

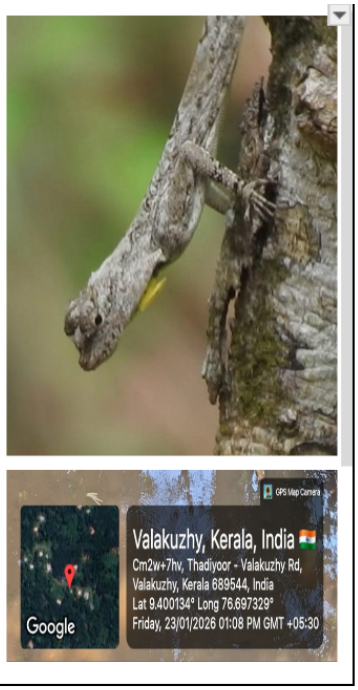

Draco with dewlap.

Draco dussumieri, Southern Flying Lizard of Western Ghats

Draco dussumieri, commonly known as the Southern Flying Lizard, is a remarkable agamid lizard endemic to the Western Ghats and associated hill ranges of Southern India. It stands as a pinnacle of evolutionary adaptation, specifically specialised for an arboreal life within the dense canopy of evergreen forests, areca nut and rubber plantations. Measuring roughly 20 to 25 centimetres in length, its most distinctive anatomical feature is the patagium, a pair of large, wing-like membranes supported by five to six greatly elongated thoracic ribs. These ribs are mobile; when the lizard is at rest, they fold against the body to facilitate camouflage, but during a leap, they are extended by specialised intercostal muscles to create a broad surface area for gliding. This allows the lizard to traverse distances of over 30 meters between trees, effectively bypassing ground-level predators and conserving energy.

The colouration of Draco dussumieri is a sophisticated example of disruptive camouflage and sexual signalling. The dorsal surface is typically a mottled, bark-like grey or olive-brown, making the lizard almost invisible when pressed flat against a tree trunk. However, this drab exterior hides vibrant secondary sexual characteristics. Males possess a vivid, lemon-yellow gular appendage (dewlap) under the chin, which they flick rapidly to signal dominance to rivals or attract mates. The underside of the patagium is similarly striking, often featuring orange or yellow hues with dark spots, visible only during flight or during specific territorial displays. Unlike the powered flight of birds or bats, Draco utilises a controlled glide, using its long, slender tail as a rudder to navigate and its forelimbs to ”steer” the leading edge of the wing membranes.

In terms of ecology and life history, Draco dussumieri is predominantly insectivorous, with a diet consisting almost exclusively of ants and small termites found on the bark of trees. Their social structure is highly territorial; a single male typically patrols a ”harem” of several trees, each inhabited by a female. While they are strictly arboreal, the life cycle necessitates a brief, perilous descent to the forest floor. Gravid females must leave the safety of the canopy to excavate a small hole in the moist soil, where they deposit a clutch of 3 to 5 eggs before

immediately returning to the trees. This vulnerable moment is the only time these ”dragons” are found on the ground. Because of their reliance on specific microclimates and tree densities, they serve as important bioindicators for the health of the Western Ghats' forest ecosystems.

Classification & Taxonomy

Order: Squamata (Lizards and Snakes)

Family: Agamidae (Agamid lizards)

Genus: Draco (The ”Gliding Dragons”)

Species: Draco dussumieri

Contents

Part I

Artificial Intelligence and Machine Learning

Introduction to Neuromorphic Computing

by Blesson George

AIRIS4D, VOL.4, NO.2, 2026

www.airis4d.com

1.1 Introduction

Conventional computers are designed to perform calculations by following a fixed sequence of instructions. They are highly efficient for numerical and logical tasks, but they struggle with problems that involve learning, adaptation, and pattern recognition. Such tasks are easily handled by the human brain, which operates with remarkable speed and extremely low power consumption.

Neuromorphic computing is an emerging computing paradigm that attempts to bridge this gap by taking inspiration from the structure and functioning of the human brain. Instead of forcing intelligence through software alone, neuromorphic computing aims to realize brain-like computation directly in hardware.

1.2 Basic Idea of Neuromorphic Computing

In the human brain, information is processed by billions of neurons that communicate through short electrical signals called spikes. Learning occurs by modifying the strength of connections, known as synapses, between neurons.

Neuromorphic computing tries to mimic this biological process using electronic circuits. Artificial neurons generate spikes, and artificial synapses store and update connection strengths. Unlike traditional computers that process data continuously, neuromorphic systems are event-driven and become active only when spikes occur.

This approach allows neuromorphic systems to perform massively parallel computation while consuming very little energy.

1.3 Why Neuromorphic Computing is Relevant

The growing interest in neuromorphic computing is mainly due to the limitations of current computing methods.

Modern artificial intelligence systems, especially deep learning models, require large datasets, powerful processors, and high energy consumption. This makes them unsuitable for many real-time and low-power applications.

Neuromorphic computing addresses these issues by:

- reducing power consumption,
- avoiding the von Neumann bottleneck by combining memory and computation,
- enabling real-time learning and decision-making.

As a result, neuromorphic systems are well suited for edge devices, robotics, and autonomous systems.

1.4 Emergence and Development

The concept of neuromorphic computing was introduced in the late 1980s by Carver Mead. He proposed building electronic circuits that behave similarly to biological neurons. His work laid the foundation for brain-inspired hardware design.

Further development of this field was driven by advances in neuroscience, microelectronics, and artificial neural networks. The introduction of spiking

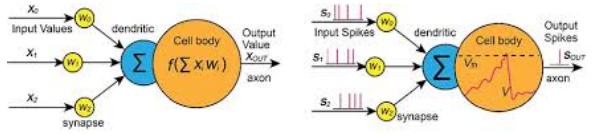

(a) The structure of artificial neurons (b) The structure of spiking neurons

Figure 1: Comparison between a biological neuron and an artificial spiking neuron used in neuromorphic computing

neural networks (SNNs) marked an important step toward more biologically realistic computation.

In recent years, neuromorphic processors such as IBM TrueNorth and Intel Loihi have demonstrated that large-scale brain-inspired hardware systems are practically feasible.

1.5 A Simple Spiking Neuron Model

Spiking neural networks are commonly used in neuromorphic computing to model the behavior of biological neurons. One of the simplest and most widely used models is the *Leaky Integrate-and-Fire (LIF)* neuron.

The change in membrane potential of a neuron is described by the equation

$$\tau \frac{dV(t)}{dt} = -V(t) + RI(t) \tag{1.1}$$

where $V(t)$ represents the membrane potential, $I(t)$ is the input current, R is the membrane resistance, and τ is the membrane time constant.

When the membrane potential reaches a fixed threshold value V_{th}, the neuron generates a spike and the potential is reset. Although simple, this model captures the essential spike-based behavior of biological neurons and is widely used in neuromorphic systems.

1.6 Difference from Conventional Computing

Neuromorphic computing differs fundamentally from traditional computing methods.

In conventional computers, memory and processing units are physically separate, and computation is mostly sequential. In contrast, neuromorphic systems integrate memory and computation and operate in a highly parallel manner.

Moreover, traditional systems use continuous-valued signals, while neuromorphic systems rely on discrete spikes. This spike-based processing enables efficient and low-power computation, especially for sensory and real-time applications.

1.7 Applications

Neuromorphic computing has potential applications in many areas, including:

- robotics and autonomous systems,
- speech and image recognition,
- edge computing and Internet of Things (IoT) devices,
- brain–machine interfaces.

These applications benefit from fast response, adaptability, and low energy consumption.

1.8 Conclusion

Neuromorphic computing is a brain-inspired computing approach that offers a promising alternative to conventional computing methods. By combining ideas from neuroscience and electronics, it enables energy-efficient and adaptive computation.

Although neuromorphic computing is still an evolving field, continued research and technological progress may allow it to play a key role in the future of artificial intelligence and intelligent machines.

About the Author

Dr. Blesson George presently serves as an Assistant Professor of Physics at CMS College Kottayam, Kerala. His research pursuits encompass the development of machine learning algorithms, along with the utilization of machine learning techniques across diverse domains.

Part II

Astronomy and Astrophysics

Plasma Physics- Cometary Plasma

by Abishek P S

AIRIS4D, Vol.4, No.2, 2026

www.airis4d.com

1.1 Introduction

Space is the immense expanse that stretches beyond Earth's atmosphere, a realm that appears empty yet is far from void. Though it is dominated by vacuum, this environment is constantly influenced by powerful forces such as radiation from stars, vast magnetic fields that thread through galaxies, and streams of charged particles emitted by the Sun known as the solar wind. These elements create a dynamic and ever-changing stage where celestial bodies interact in remarkable ways. Among them, comets stand out as natural laboratories of physics. Composed of ice, dust, and organic compounds, comets preserve material from the early solar system, offering scientists a glimpse into its primordial past. As they travel through space and approach the Sun, the heat and solar wind trigger sublimation of their icy cores, producing glowing comas and long, luminous tails. These processes reveal fundamental principles of thermodynamics, plasma physics, and magnetohydrodynamics in action. Moreover, the organic molecules found within comets provide tantalizing clues about the origins of life, suggesting that they may have played a role in delivering essential building blocks to Earth. In this way, comets are not merely wandering icy bodies but dynamic testbeds where the laws of physics and chemistry unfold on a cosmic scale.

When sunlight and the solar wind interact with the gases released from a comet, they trigger a process of ionization in which neutral atoms and molecules are transformed into charged particles, creating what is known as cometary plasma, a mixture of ions and electrons. This plasma is not static; it is continuously influenced and sculpted by the solar wind, which streams outward from the Sun at high speeds. As a result, the comet develops a distinct plasma tail that always points directly away from the Sun, regardless of the comet's orbital path or direction of travel. This phenomenon illustrates the powerful influence of solar radiation and charged particle flows on matter in space. By studying cometary plasma, we get valuable insights not only into the physical behaviour and evolution of comets but also into broader plasma processes that occur throughout the universe. These investigations shed light on how radiation and magnetic fields interact with matter, offering clues about the dynamics of planetary magnetospheres, the behaviour of stellar winds, and even the fundamental physics of plasma that governs much of the cosmos [1,2].

1.2 Formation of Cometary Plasma

The formation of cometary plasma is a multi-stage process that vividly demonstrates the interaction between solar energy and the primordial materials of a comet. It begins with nucleus outgassing, which occurs as the comet approaches the Sun. The nucleus, a solid core composed of frozen volatiles such as water ice, carbon dioxide, and carbon monoxide, is heated by solar radiation. This heating causes sublimation, the direct transition of these ices into gas releasing jets of vapor along with entrained dust particles. These outgassing events can be highly localized, producing geyser-like eruptions from cracks and vents on the comet's surface, and they intensify as the comet moves closer to the Sun.

The released gases expand outward to form the coma, a vast, diffuse envelope surrounding the nucleus. The coma acts as a temporary atmosphere for the comet, composed primarily of neutral molecules and dust grains. Its size can reach tens of thousands of kilometres across, making it the most visible part of the comet when observed from Earth. Within this coma, the density of particles is still extremely low compared to Earth's atmosphere, but it is sufficient to interact with incoming solar radiation and charged particles.

Next comes ionization, a critical step in plasma formation. Ultraviolet photons from the Sun and energetic particles carried by the solar wind collide with the neutral molecules in the coma, stripping away electrons and creating ions. This process transforms portions of the neutral gas into a plasma, a dynamic mixture of positively charged ions and free electrons. Because plasma is highly responsive to electromagnetic forces, it becomes entrained in the solar wind flow. The interaction between the solar wind and the cometary plasma generates a distinct plasma tail, which always points directly away from the Sun, regardless of the comet's orbital trajectory. This tail can stretch millions of kilometres into space, serving as a visible marker of plasma dynamics in action.

Finally, dust contribution adds further complexity to the plasma environment. Alongside gases, dust grains are continuously ejected from the nucleus during outgassing. These grains can become electrically charged through photoionization or collisions with plasma particles. Once charged, they interact with the surrounding plasma and magnetic fields, influencing the structure and behaviour of both the dust tail and the plasma tail. Dust particles also scatter sunlight, contributing to the comet's brightness, and their interactions with plasma can lead to phenomena such as turbulence, recombination, and variations in tail morphology [2].

Taken together, these stages of outgassing, coma development, ionization, and dust-plasma interactions illustrate how comets act as natural laboratories for studying fundamental physical processes. They reveal the interplay of thermodynamics, radiation physics, plasma dynamics, and electromagnetic forces in a way that is observable on a cosmic scale. By examining cometary plasma, scientists gain not only a deeper understanding of cometary behaviour but also valuable insights into universal plasma processes that shape planetary atmospheres, stellar winds, and the broader dynamics of the solar system.

The plasma components of a comet are diverse and intricately connected, each contributing to the dynamic environment that surrounds the nucleus and extends into the comet's tails. At the core of this system is the neutral gas, which originates from the sublimation of volatile ices such as water (H_2O), carbon dioxide (CO_2), and carbon monoxide (CO) as the comet approaches the Sun. These gases expand outward to form the coma, a vast neutral atmosphere that serves as the reservoir for plasma creation. The neutral molecules are the starting point for ionization processes, and their abundance determines the density and composition of the resulting plasma.

Through the action of solar ultraviolet radiation and collisions with energetic solar wind particles, these neutral molecules undergo ionization, producing a variety of ions. Common examples include H_2O^+, CO^+, and $CO^+{}_2$, along with other molecular ions formed through fragmentation and chemical reactions within the coma. These ions are highly responsive to electromagnetic forces, and once created, they are swept up by the solar wind, contributing to the formation of the plasma tail. The ions also participate in complex chemical pathways, recombining with electrons or interacting with dust grains, which further modifies the plasma's structure and behaviour [3].

Alongside ions, electrons are generated during the ionization process. These free electrons are extremely light and mobile compared to ions, allowing them to move quickly through the plasma. Their mobility makes them essential for maintaining charge neutrality and for driving electrical currents within the cometary environment. Electrons also play a role in exciting neutral molecules, leading to the emission of characteristic spectral lines that allow scientists to study the composition of the comet remotely. In addition, electron interactions can produce instabilities and waves within the plasma, adding to its dynamic nature.

Finally, dust particles released from the comet's nucleus add another layer of complexity to the plasma system. These grains, ranging in size from microscopic specks to larger fragments, can become electrically charged through photoionization or collisions with plasma particles. Once charged, dust grains interact with the surrounding plasma and magnetic fields, influencing currents and wave activity. Their presence can alter the distribution of ions and electrons, create turbulence, and contribute to the splitting or bending of cometary tails. Dust also scatters sunlight, enhancing the comet's brightness and making its tails visible from Earth, while simultaneously serving as active participants in plasma dynamics.

Together, these components such as neutral gas, ions, electrons, and dust particles form a highly interactive and evolving plasma environment. The balance between them determines the structure of the comet's coma and tails, while their interactions provide a natural laboratory for studying fundamental processes such as ionization, recombination, electromagnetic coupling, and wave propagation.

1.3 Plasma Structures around Comets

The plasma structures around comets are among the most striking and scientifically rich features in the solar system, arising from the interplay between cometary material and the solar wind. At the core of these structures lies the coma plasma, which forms when neutral gases released from the comet's nucleus are ionized by solar ultraviolet radiation and energetic particles. This ionized region envelops the nucleus, creating a dense, glowing atmosphere of ions and electrons that serves as the foundation for further plasma interactions. The coma plasma is not static; it expands outward and interacts continuously with the solar wind, setting the stage for the development of large-scale plasma tails and boundaries.

One of the most distinctive features is the ion tail, also known as the plasma tail. Composed of ions and electrons swept away by the solar wind, this tail always points directly away from the Sun, regardless of the comet's orbital path. Its orientation is dictated by the solar wind's flow and the interplanetary magnetic field, which guide the charged particles into long, narrow streams that can extend millions of kilometres into space. The ion tail often appears bluish due to the emission of light from ionized carbon monoxide and other molecules, and its dynamic behaviour such as sudden disconnections or kinks provides direct evidence of solar wind variability and magnetic reconnection events. In contrast, the dust tail is formed by solar radiation pressure acting on dust grains released from the nucleus. Unlike the plasma tail, the dust tail curves along the comet's trajectory, reflecting the combined influence of the comet's motion and solar radiation. Dust grains scatter sunlight, making this tail bright and often yellowish, and its structure reveals information about particle sizes and the rate of dust release.

Beyond these visible tails, comets also exhibit complex plasma boundaries that mark the transition zones between cometary plasma and the solar wind. The ionopause is the boundary where the dense plasma of the coma meets the incoming solar wind, acting as a shield that separates the comet's internal plasma environment from external influences. This boundary is shaped by pressure balance between the cometary outflow and the solar wind, and its position can shift depending on the comet's activity level and solar wind conditions. Ahead of the comet, the bow shock forms as the supersonic solar wind slows down and deflects around the expanding coma. This shock region is analogous to those found around planets with atmospheres or magnetospheres, and it provides a natural laboratory for studying shock physics and energy transfer in plasma systems. Additionally, comets can develop magnetotail-like structures, elongated regions of plasma shaped by the solar wind's magnetic field lines. These structures resemble planetary magnetotails and demonstrate how even small bodies like comets can generate large-scale plasma phenomena through their interaction with the solar wind [4].

Together, these plasma structures such as coma plasma, ion tail, dust tail, ionopause, bow shock, and magnetotail-like regions illustrate the complexity of cometary environments and their role as natural laboratories for plasma physics. They

reveal fundamental processes such as ionization, electromagnetic coupling, shock formation, and magnetic field interactions, all of which are central to understanding not only comets but also the broader dynamics of the solar system and interstellar space.

1.4 Plasma Processes

The plasma processes around comets are intricate and unfold in multiple regimes, reflecting the transition from dense, collision-dominated environments near the nucleus to tenuous, collisionless plasma farther out in space. Close to the nucleus, the collisional regime dominates because the density of neutral gas released by sublimation is relatively high. In this region, frequent collisions occur between neutral molecules and newly formed ions, leading to energy transfer, recombination, and chemical reactions that continuously alter the plasma composition. These collisions also slow down particle motion, creating a more fluid-like behaviour where the plasma is tightly coupled to the neutral gas. This inner region is crucial for understanding how cometary atmospheres evolve and how the initial plasma is generated.

As the plasma expands outward into space, the density of particles decreases significantly, and the system transitions into a collisionless regime. Here, collisions between particles become rare, and collective electromagnetic effects dominate. Instead of direct collisions, plasma behaviour is governed by wave-particle interactions, instabilities, and long-range electromagnetic forces. This regime resembles the plasma environments found in planetary magnetospheres and the solar wind itself, making comets excellent natural laboratories for studying universal plasma physics. In this region, charged particles can be accelerated by electric fields, trapped by magnetic fields, and influenced by plasma waves, leading to highly dynamic structures such as the plasma tail.

A particularly important process in cometary plasma is charge exchange, where solar wind ions interact with neutral atoms or molecules from the comet's coma. In this interaction, a solar wind ion captures an electron from a neutral particle, becoming a slower-moving neutral atom, while the neutral particle becomes ionized. This process alters the composition of the plasma, introduces new ion species, and modifies the energy distribution of particles. Charge exchange also produces energetic neutral atoms that can escape the plasma environment, providing valuable diagnostic signals for spacecraft observations. It is one of the key mechanisms by which the solar wind and cometary material exchange energy and momentum.

Another fundamental aspect is the interaction with magnetic fields. The solar wind carries the interplanetary magnetic field (IMF), which couples directly with the cometary plasma. This coupling generates turbulence, induces electric currents, and shapes large-scale structures such as bow shocks and magnetotail-like regions. The magnetic field interaction is responsible for bending and stretching the plasma tail, and it can trigger reconnection events where magnetic field lines break and reconnect, releasing energy and causing sudden changes in tail morphology. These processes mirror those observed in planetary magnetospheres, highlighting the universality of plasma-magnetic field interactions.

Finally, comets are rich sources of plasma waves, which arise from instabilities in the ionized environment. Electrostatic waves, driven by fluctuations in charge density, and electromagnetic waves, influenced by magnetic field variations, propagate through the plasma. These waves can accelerate particles, redistribute energy, and create turbulence within the cometary environment. For example, ion cyclotron waves and Langmuir waves have been detected near comets, providing direct evidence of plasma instabilities. Such waves not only shape the local plasma dynamics but also serve as diagnostic tools for understanding the conditions within the comet's coma and tail.

The plasma processes around comets' collisional and collisionless regimes, charge exchange, magnetic field interactions, and plasma wave propagation represent a complex interplay of physics that bridges small-scale particle interactions with large-scale electromagnetic phenomena. Studying these processes in detail allows us to uncover fundamental principles

of plasma behaviour that apply not only to comets but also to planetary atmospheres, stellar winds, and astrophysical plasmas throughout the universe.

1.5 Significance of Studying Cometary Plasma

The scientific importance of cometary plasma lies in its ability to connect small-scale processes around comets with large-scale questions about the solar system, astrophysics, and plasma physics. One of the most significant aspects is its role in understanding solar system evolution. Comets are considered to be among the most primitive bodies, preserving volatile compounds such as water, carbon dioxide, and carbon monoxide from the early solar nebula. When these volatiles are released and ionized to form plasma, we can analyse their composition and isotopic ratios. This helps trace the origin and distribution of volatiles across the solar system, offering clues about how planets acquired their atmospheres and oceans, and whether comets may have contributed to the delivery of life-essential molecules to Earth. In this way, cometary plasma serves as a direct link to the chemical and physical conditions of the solar system's formation billions of years ago.

Cometary plasma also provides an astrophysical analogy, functioning as a natural laboratory for plasma processes that occur on vastly different scales in stars, nebulae, and galaxies. The ionization, charge exchange, and magnetic field interactions observed around comets mirror phenomena seen in stellar winds, interstellar clouds, and galactic plasmas. For example, the bow shock formed ahead of a comet resembles shocks around supernova remnants, while plasma instabilities in cometary tails are similar to those in astrophysical jets. By studying comets up close, researchers can test theories of plasma physics under conditions that are otherwise difficult to replicate in laboratories, thereby gaining insights into universal processes that govern the cosmos.

In addition, cometary plasma plays a crucial role in space weather studies. The interaction between the solar wind and cometary material creates boundaries such as bow shocks, ionopauses, and magnetotail-like structures, which are analogous to those found around planets. Observing these boundaries in comets helps scientists understand how solar wind shapes planetary magnetospheres and atmospheres, and how energy and momentum are transferred across plasma interfaces. This knowledge is vital for predicting and mitigating the effects of space weather on Earth, including disruptions to satellites, communication systems, and power grids. Comets, therefore, act as natural probes of solar wind behaviour, offering real-time case studies of how plasma boundaries form and evolve under varying solar conditions.

Finally, cometary plasma contributes to fusion and plasma physics research by providing real-world examples of both collision-dominated and collisionless regimes. Near the nucleus, the plasma is dense enough that collisions between neutrals and ions dominate, creating a fluid-like environment. Farther out, the plasma becomes tenuous and collisionless, where collective electromagnetic effects and wave-particle interactions govern its behaviour. This transition between regimes is of great interest to laboratory plasma research, especially in the context of controlled nuclear fusion, where understanding instabilities, turbulence, and energy transport is critical. Observations of plasma waves, charge exchange, and magnetic reconnection in comets provide natural experiments that inform the design and interpretation of laboratory plasma systems.

The study of cometary plasma is important because it bridges planetary science, astrophysics, and applied plasma physics. It helps reconstruct the history of the solar system, serves as an analogy for cosmic plasma processes, enhances our understanding of space weather, and informs laboratory research aimed at harnessing fusion energy. By examining comets, scientists gain access to a wealth of information about how matter and radiation interact across scales, making these icy wanderers invaluable laboratories for exploring the fundamental physics of the universe.

References

[1] Goetz, C., Gunell, H., Volwerk, M. et al. Cometary plasma science. Exp Astron **54**, 1129–1167 (2022). https://doi.org/10.1007/s10686-021-09783-z

[2] Miyamoto, K. (1979). "Plasma physics for nuclear fusion", Wallis, M. K. (1967). The physics of cometary plasma. Planetary and Space Science, 15

[3] Schmidt, H. U., Wegmann, R., Huebner, W. F., & Boice, D. C. (1988). Cometary gas and plasma flow with detailed chemistry. Computer Physics Communications, 49(1), 17-59.

[4] Cravens, T. E. (1989). Cometary plasma boundaries. Advances in Space Research, 9(3), 293-304.

About the Author

Abishek P S is a Research Scholar in the Department of Physics, Bharata Mata College (Autonomous) Thrikkakara, kochi. He pursues research in the field of Theoretical Plasma physics. His works mainly focus on the Nonlinear Wave Phenomenons in Space and Astrophysical Plasmas.

Black Hole Stories-24
Some Back Hole Mergers From Gravitational Wave Detector Observing Runs O1 and O2

by Ajit Kembhavi

AIRIS4D, VOL.4, NO.2, 2026

www.airis4d.com

2.1 Inter-University Centre for Astronomy and Astrophysics

In this story we will consider some of the binary black holes detected during the observing runs O1 and O2. These examples are indicative of the variety of binary mergers found in these two runs.

2.2 The First Observing Run O1

The first observing run of the aLIGO detectors began on September 12, 2015 and continued until January 19, 2016. During this run a total of three black hole binary merger events were detected, including the very first detection GW150914, which we have described in BHS-21. Here we will describe another black hole binary from O1,GW151226.

2.2.1 GW151226:

This is again a black hole binary source which merged to form a single black hole. It was detected, as it name implies, on December 26, 2015, i.e., on Boxing Day, which is the day following Christmas Day. It was observed at 03:38:53 UTC by the LIGO detectors at Livingston and Hanford, the inferred merger time at Livingston being one millisecond earlier than at Hanford.

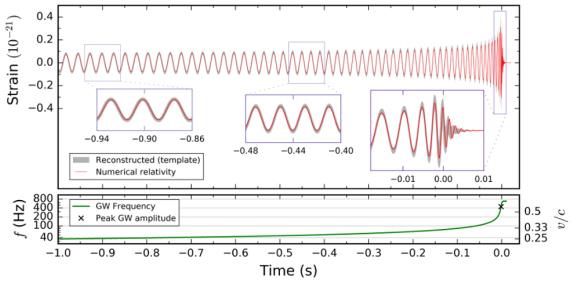

Figure 1: Black hole merger eventGW151226. Upper panel: The waveform as estimated from theory is shown. The inset boxes show details of the model in three time intervals, together with numerically calculated models for the event. Lower panel: the decrease in separation as the component spiral in, and the consequent increase in their relative velocity are shown. Image Credit: B. P. Abbott et al. Physical Review Letters volume 116, p. 241103, 2016.

The signal in this case was weaker than in the case of GW150914, and the event was spread over one second, compared to the 0.2 second spread of the earlier detection. As a result, it was more difficult to detect the signal, and a special technique known as *matched filtering* had to be used. This was first developed in the context of gravitational wave detection by Bangalore Sathyaprakash and Sanjeev Dhurandhar. During the 1s that the signal was detected, it went through 55 cycles, which are shown in Figure 1. The height of the peaks increases with time, as does the frequency of the signal, since the two components of the binary spiral towards each other due to the energy loss to gravitational

wave emission. The peak frequency reached is 450 Hz, which means that the two components approach each other very closely without being destroyed, and must therefore be black holes. The ringdown to single black hole formation is clearly seen in the inset on the extreme right. Calculations show that the two black holes in the binary are of about 14.2 and 7.5 Solar masses, which makes them significantly less massive than the black holes in GW150914. The mass of the spinning black hole produced through the merger is about 20.8 Solar masses, so that about a Solar mass is lost from the system due to the emission of gravitational waves. The source is at a distance of about 1.4 billion light years (430Mpc) from us.

2.3 The Second Observing Run O2

After detector and system upgradation, the second observing run O2 began on September 30, 2016 and continued until August 25, 2017. During this period eight detections were made, including the binary neutron star merger GW170817, which was also detected at electromagnetic wavelengths. We have described the source in detail in BHS-23. We will now describe four black hole mergers of those detected during O2, GW170104, GW170608, GW170729 and GW170814.

GW170104: This source was detected on January 4, 2017, and was the first source to be found after the start of the second observing run. Detailed analysis showed that it was a black hole binary which merged to form a single black hole, with masses of the two components in the initial binary system being 31.2 and 19.4 Solar masses. The final black hole has mass 48.7 Solar masses, so that about two Solar masses was lost from the system upon merger The source is at a distance of about 2.9 billion light years (890 Mpc).

GW170608: This source was detected on June 8, 2017. It was again a black hole binary which merged to form a single black hole. The masses of the two components in the binary system were 12 and 7 Solar masses respectively. About one Solar mass was radiated away during the merger. The source is at a distance of 1.1 billion light years (340 Mpc). The masses of the black holes in this source were considerably smaller than the black hole component masses found in other sources observed until this discovery.

GW170729: This source was the most distant and luminous source observed in O2. The merger occurred about 5 billion years ago, that is before the formation of the Solar system, and about 5 Solar masses were lost from the system in the form of gravitational waves emitted during the merger.

GW170814: This is a black hole binary detected on August 14, 2017, with the two components found to have about 30.5 and 25.3 Solar masses, while the mass of the black hole after the merger is about 53.2 Solar masses. The source is at a distance of about 1.8 billion light years (560 Mpc) from us. The novelty in the detection is that for the first time the source was observed by three detectors: the two advanced LIGO detectors at Livingston and Hanford and the advanced VIRGO detector in Italy and was the first detection by VIRGO. This enabled the direction of the source in the sky to be limited to a region of 60 square degrees. This area is much smaller than the possible regions in the sky for the other sources, which were observed only by the two advanced LIGO detectors. Using observations from the three detectors it has been possible to measure gravitational wave polarisation. These measurements are fully consistent with the prediction of general relativity, and are not consistent with results expected from other competing theories of gravity. This detection was followed in three days by the neutron star binary **GW170817**, which have discussed in detail in BHS-23.

2.4 Black Hole Masses From O1 and O2

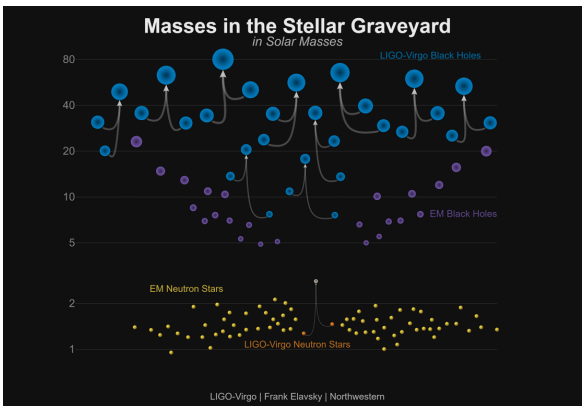

Figure 2: The 10 black hole binaries and one neutron star binary whose mergers were observed in observing runs O1 and O2. Details of the figure are explained in the text. Image Credit: LIGO/Frank Elavsky/Northwestern. This diagram as also used in BHS-1.

The ten black hole binary merger and one neutron star binary were detected in the observing runs O1 and O2 are shown schematically in Figure 2. For each black hole merger, a set of three blue circles indicate the mass of each component of the binary before merger, and the mass of the remnant post-merger. The purple circles indicate the mass of black holes detected as a component of an X-ray binary system. These black holes are detected through X-ray and optical observations of the binary systems, through electromagnetic means. The purple circles together have been labelled as EM black holes, while the blue circles are labelled as LIGO-Virgo black holes. It is seen from the diagram that the masses of the LIGO-Virgo black holes in many cases are significantly larger than the masses of the EM black holes. The reason is that the larger the black hole mass, the greater is the gravitational wave luminosity of the system and shorter is the time over which the signal is spread out at the merger. This makes the signal more easily detectable over the background noise. It is expected that there will in fact be many more low mass black hole binaries than the high mass binaries which have been detected so far. The lower mass systems will be detected with increased sensitivity of the gravitational wave detectors.

Each yellow circle indicates the mass of a neutron star, which was electromagnetically detected as the compact component of an X-ray binary system. The EM neutron star masses in the figure are all well below the maximum mass limit for neutron stars, which is about three Solar masses. In the case of the binary neutron star merger event GW170817 shown in the figure, the mass of the remnant is estimated to be 2.82 Solar masses, which is at the upper end of the permissible mass of neutron stars. The remnant could very well be a black hole. In that case it would be the only black hole which is in the mass range of 2-5 Solar masses. This region is known as the *mass gap* region because of the lack of black holes in it. Binary black holes with pre- or post-merger component mass in this region would be difficult to detect through their gravitational wave emission, given the present sensitivity of the detectors, and none has been found through electromagnetic observations. It is possible of course that there are no black holes, or at least relatively few black holes, with mass in this region. That would be a very interesting astrophysical fact which would need to be carefully examined and explained.

In the next story we will consider binary mergers detected in O3 and O4.

About the Author

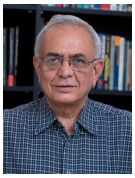

Professor Ajit Kembhavi is an emeritus Professor at Inter University Centre for Astronomy and Astrophysics and is also the Principal Investigator of the Pune Knowledge Cluster. He was the former director of Inter University Centre for Astronomy and Astrophysics (IUCAA), Pune, and the International Astronomical Union vice president. In collaboration with IUCAA, he pioneered astronomy outreach activities from the late 80s to promote astronomy research in Indian universities.

X-ray Astronomy: Theory

by Aromal P

AIRIS4D, VOL.4, NO.2, 2026

www.airis4d.com

3.1 Introduction

In the previous article we have discussed about the Different Mechanism that produces X-rays! As the second article in the series in this article we will be discussing about different X-ray sources and the main mechanism in primarily acting on each system.

3.2 Stellar Corona

While stars like our Sun emit most of their energy in the optical band, they possess hot outer atmospheres called corona that radiate in X-rays.

- Mechanism: The heating of the stellar corona is driven by the stressing and relaxation of magnetic field loops anchored in the star's photosphere. When these magnetic loops reconnect (magnetic reconnection), they release stored energy, heating the coronal plasma to temperatures of nearly million kelvin. The hot plasma emits X-rays primarily through thermal bremsstrahlung and atomic line transitions. Young, rapidly rotating stars can exhibit X-ray luminosities 4 times magnitudes higher than the Sun due to more vigorous magnetic dynamos.

3.3 Supernova Remnants (SNRs)

When massive stars explode, they leave behind expanding shock waves that heat the interstellar medium (ISM) and accelerate particles.

- Mechanism: SNRs produce X-rays via two distinct processes:

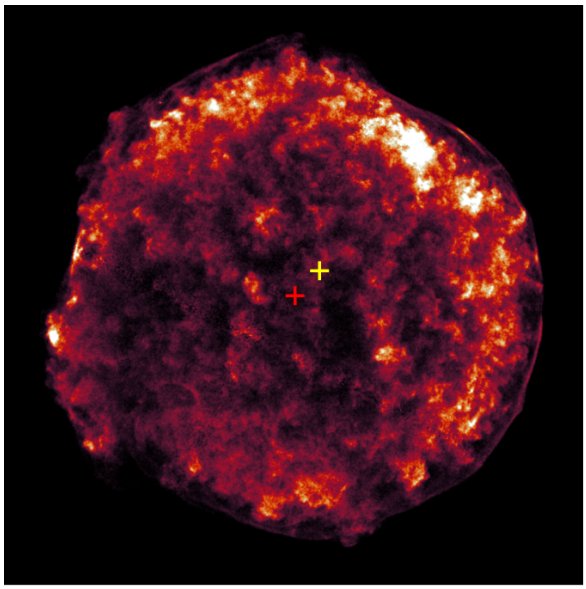

Figure 1: X-ray image of Tycho SNR in 1.2-4.0 keV. (Image credit : Petruk et al. 2025)

1. Thermal Emission (Shell-type): The supernova shock wave sweeps up the surrounding ISM, heating it to temperatures of million Kelvin. This gas emits thermal X-rays via bremsstrahlung.
2. Non-Thermal Emission (Plerions) In remnants like the Crab Nebula, a central pulsar accelerates electrons to relativistic speeds. These electrons spiral in the magnetic field, emitting synchrotron radiation that extends into the X-ray band.

3.4 X-ray Binaries (XRBs)

These are the brightest X-ray sources in the galaxy, consisting of a compact object accreting matter from a companion star.

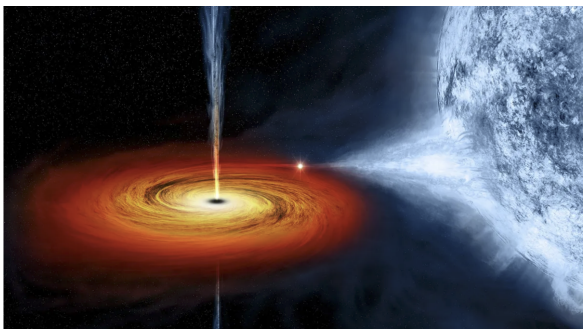

Figure 2: An artist's impression of the Cygnus X-1 X-ray binary, which features a black hole stripping material from a companion star, and the material forming a hot accretion disk. (Image credit: NASA/CXC/M. Weiss)

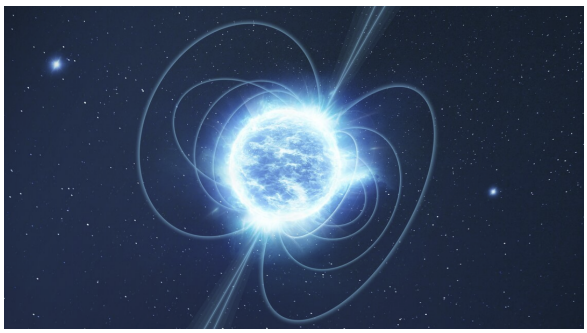

Figure 3: an artist's impression of a magnetar. (Image credit: ESA)

3.4.1 Neutron Star Binaries

- Mechanism: Matter flowing from the companion forms an accretion disk. As it spirals inward, viscosity heats the disk to X-ray temperatures. When this material crashes onto the solid surface of the neutron star, its kinetic energy is thermalized, releasing intense X-rays. Additionally, accumulated matter can undergo thermonuclear runaway, causing Type I X-ray bursts.

3.4.2 Black Hole Binaries

- Mechanism: Similar to neutron stars, black holes accrete via a disk. However, lacking a solid surface, the X-rays originate entirely from the inner accretion disk and a hot corona of electrons above it. The emission is characterized by a soft thermal component from the disk and a hard power-law component produced by Inverse Compton scattering of disk photons by hot coronal electrons.

3.5 Isolated Neutron Stars (INS)

Not all neutron stars are in binary systems. Some are isolated, radiating X-rays through cooling or magnetic activity.

- Mechanism:
  1. Cooling (Thermally Emitting INS): Young neutron stars retain immense heat from their formation. They emit soft X-rays purely as a result of blackbody cooling from their surface having a temperature about a million Kelvin.
  2. Magnetars: These are isolated neutron stars with ultra-strong magnetic fields ($B \sim 10^{14}$–10^{15} G). Their X-ray emission is powered by the decay of their internal magnetic field, which heats the crust and magnetosphere, rather than rotational energy or accretion.

3.6 Active Galactic Nuclei (AGN)

AGN are supermassive black holes (10^6–$10^9 M_\odot$) at the centers of galaxies, actively consuming matter.

- Mechanism The primary X-ray continuum in AGN is produced by Inverse Compton scattering. UV photons from the cool accretion disk are up-scattered to X-ray energies by a hot corona of electrons surrounding the black hole. This radiation can also reflect off the accretion disk, producing fluorescence lines, most notably the Iron Kα line at 6.4 keV.

3.7 Galaxy Clusters

Clusters are the largest gravitationally bound structures, containing hundreds of galaxies immersed in a vast cloud of hot gas called the Intracluster Medium (ICM).

- Mechanism: The ICM is heated to temperatures of order of tens of million Kelvin by the gravitational potential energy of the cluster's dark

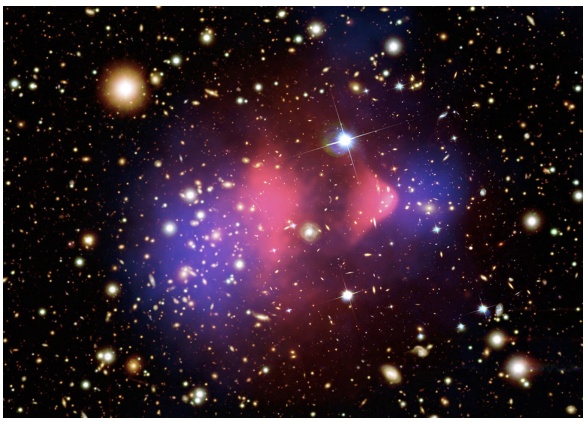

Figure 4: Composite image shows the galaxy cluster 1E 0657-556, also known as the "bullet cluster." (Image credit: ESA)

matter halo. At these temperatures, the hydrogen and helium are fully ionized. The electrons are deflected by atomic nuclei, emitting X-rays via thermal bremsstrahlung. This mechanism makes galaxy clusters the most luminous extended X-ray sources in the universe.

The author is mostly focused on Neutron Star X-ray Binaries we will be discussing about the theory behind such system shortly and will extend to other system as well in the upcoming articles.

Reference:

- Rosner, R., Golub, L., & Vaiana, G. S. (1985). On stellar X-ray emission. *Annual Review of Astronomy and Astrophysics*, 23, 413-452.
- Reynolds, S. P. (2008). Supernova Remnants at High Energy. *Annual Review of Astronomy and Astrophysics*, 46, 89-126.
- Lewin, W. H. G., & van der Klis, M. (Eds.). (2006). *Compact Stellar X-ray Sources*. Cambridge University Press.
- Shakura, N. I., & Sunyaev, R. A. (1973). Black holes in binary systems. Observational appearance. *Astronomy and Astrophysics*, 24, 337-355.
- Yakovlev, D. G., & Pethick, C. J. (2004). Neutron Star Cooling. *Annual Review of Astronomy and Astrophysics*, 42, 169-210.
- Kaspi, V. M., & Beloborodov, A. M. (2017). Magnetars. *Annual Review of Astronomy and Astrophysics*, 55, 261-301.
- Haardt, F., & Maraschi, L. (1991). A two-phase model for the X-ray emission from Seyfert galaxies. *The Astrophysical Journal*, 380, L51-L54.
- Sarazin, C. L. (1986). X-ray emission from clusters of galaxies. *Reviews of Modern Physics*, 58(1), 1-115.

About the Author

Aromal P is a research scholar in Department of Astronomy, Astrophysics and Space Engineering (DAASE) in Indian Institute of Technology Indore. His research mainly focuses on studies of Thermonuclear X-ray Bursts on Neutron star surface and its interaction with the Accretion disk and Corona.

The Birth of Stars: Physical Processes Governing Stellar Formation

by Sindhu G

AIRIS4D, Vol.4, No.2, 2026

www.airis4d.com

4.1 Introduction

Stars are the primary engines of energy production and chemical enrichment in the Universe. Through nuclear fusion, they generate radiation, synthesize heavy elements, and shape their environments via winds, radiation, and supernova explosions. Understanding how stars form is therefore essential for explaining the structure and evolution of galaxies, the initial mass function, and the origin of planetary systems.

Star formation proceeds under highly selective physical conditions within molecular clouds, with only a fraction of the available gas ultimately incorporated into stellar objects. The masses of newly formed stars cover a wide range, extending over several orders of magnitude. Stellar birth is initiated when cold interstellar gas becomes gravitationally unstable and undergoes collapse, leading to the formation of self-gravitating condensations that eventually reach the temperatures and densities required for hydrogen fusion in their cores. This sequence of events encompasses spatial scales ranging from tens of parsecs in giant molecular clouds to stellar radii, rendering star formation an intrinsically multi-scale and complex phenomenon.

4.2 Giant Molecular Clouds

Stars form almost exclusively within giant molecular clouds (GMCs), which represent the coldest and densest phase of the interstellar medium. GMCs typically have masses of 10^4–$10^6\,M_\odot$, sizes of tens of parsecs, and temperatures of 10–20 K. Their composition is dominated by molecular hydrogen, with helium and trace amounts of heavier molecules and dust.

Because molecular hydrogen lacks a permanent dipole moment, GMCs are observed indirectly through emission from tracer molecules such as CO and through thermal emission from dust grains. Dust plays a crucial role in star formation by shielding cloud interiors from ultraviolet radiation, enabling molecular survival and efficient cooling. Cooling allows the gas to reach low temperatures, reducing thermal pressure and promoting gravitational collapse.

4.3 Dense Cores and Cloud Fragmentation

Star formation within GMCs is highly structured. Stars do not form uniformly but instead originate in dense subregions known as clumps and cores. Dense cores typically have sizes of ~ 0.1 pc, masses of a few solar masses, and densities exceeding 10^4 cm^{-3}. These cores represent the immediate progenitors of individual stars or small multiple systems.

The fragmentation of molecular clouds is influenced by gravity, turbulence, and magnetic fields. Supersonic turbulence generates density fluctuations that may collapse if they exceed a critical threshold. Magnetic fields provide additional support against

gravity, while ambipolar diffusion allows neutral gas to drift relative to magnetic field lines, enabling collapse on longer timescales. The interplay of these processes determines the mass distribution of forming stars.

4.4 Gravitational Instability

Gravitational collapse begins when a region of gas becomes unstable to its own gravity. This condition is commonly described by the Jeans criterion, which defines a critical mass above which thermal pressure can no longer support a cloud against collapse. The Jeans mass decreases with decreasing temperature and increasing density, favouring collapse in cold, dense environments.

External triggering mechanisms can also promote collapse. Supernova shock waves, expanding H II regions, and spiral density waves can compress molecular gas, increasing its density and driving regions above the critical threshold for gravitational instability. These processes connect star formation to galactic-scale dynamics.

4.5 Protostar Formation

As collapse proceeds, dense cores contract and form central condensations known as protostars. During this stage, the protostar is deeply embedded within its natal envelope and is optically obscured at visible wavelengths. Its emission is dominated by infrared and sub-millimetre radiation produced by heated dust and gas.

The luminosity of a protostar is primarily powered by the conversion of gravitational potential energy into heat as material accretes onto the central object. Nuclear fusion has not yet begun, and the internal structure is governed by hydrostatic balance between gravity and thermal pressure. Protostellar evolution during this phase depends strongly on the accretion rate and surrounding environment.

4.6 Accretion Disks

Conservation of angular momentum during collapse naturally leads to the formation of a circumstellar accretion disk. These disks regulate the flow of material from the envelope onto the protostar and play a central role in determining stellar mass. They also provide the initial conditions for planet formation.

Accretion is often episodic rather than steady, leading to luminosity variability in young stellar objects. Disk instabilities and interactions with magnetic fields can strongly influence accretion efficiency and timescales.

4.7 Jets, Outflows, and Feedback

Accreting protostars commonly drive bipolar jets and molecular outflows. These highly collimated structures are thought to be launched by magneto-centrifugal processes operating in the inner regions of the accretion disk. Jets remove excess angular momentum, enabling continued accretion, while injecting energy and momentum into the surrounding medium.

Observationally, jets are traced by Herbig–Haro objects, which mark shock fronts produced as outflows interact with the interstellar medium. Feedback from radiation, winds, and outflows disperses the remaining envelope material and helps regulate star formation efficiency.

4.8 Pre-Main-Sequence Evolution

Once the protostellar envelope is largely dispersed, the object enters the pre-main-sequence (PMS) phase. Low-mass stars appear as T Tauri stars, characterized by strong magnetic activity and variability, while intermediate-mass stars evolve as Herbig Ae/Be objects. During this stage, stars contract quasi-hydrostatically and follow characteristic evolutionary tracks in the Hertzsprung–Russell diagram.

Hydrogen fusion begins when the central temperature reaches approximately 10^7 K, marking the star's arrival on the zero-age main sequence (ZAMS).

4.9 Timescales and Mass Dependence

Star formation timescales depend strongly on stellar mass. Low-mass stars typically form over 10^6–10^7 yr, whereas massive stars may reach the main sequence in less than 10^5 yr. In the most massive cases, nuclear burning may begin while accretion is still ongoing.

Massive stars exert strong radiative and mechanical feedback, ionizing nearby gas and driving powerful winds that can suppress or trigger further star formation. This feedback shapes the evolution of star-forming regions and young clusters.

4.10 Observational Constraints

Advances in infrared, sub-millimetre, and time-domain astronomy have revolutionized the study of stellar birth. Observations from missions such as *Spitzer* and *JWST*, combined with ground-based facilities, reveal embedded protostars, accretion disks, and molecular outflows. Variability studies provide additional constraints on accretion processes and magnetic activity in young stars.

4.11 Conclusions

The birth of stars is a complex and hierarchical process governed by gravity, thermodynamics, turbulence, magnetic fields, and feedback. From the fragmentation of molecular clouds to the emergence of main-sequence stars, stellar birth shapes the evolution of galaxies and sets the initial conditions for planetary systems. Continued multi-wavelength observations and theoretical modelling are essential for achieving a complete understanding of this fundamental astrophysical process.

References:

- Theory of Star Formation
- MASS, LUMINOSITY, AND LINE WIDTH RELATIONS OF GALACTIC MOLECULAR CLOUDS
- The Big Problems in Star Formation: the Star Formation Rate, Stellar Clustering, and the Initial Mass Function
- Molecular Clouds in the Milky Way
- FROM PRE-STELLAR CORES TO PROTOSTARS: THE INITIAL CONDITIONS OF STAR FORMATION
- Control of star formation by supersonic turbulence
- The Stability of a Spherical Nebula
- Star formation in molecular clouds: observation and theory
- An internet server for pre-main sequence tracks of low- and intermediate-mass stars

About the Author

Sindhu G is a research scholar in the Department of Physics at St. Thomas College, Kozhencherry. She is doing research in Astronomy & Astrophysics, with her work primarily focusing on the classification of variable stars using different machine learning algorithms. She is also involved in period prediction for various types of variable stars—especially eclipsing binaries—and in the study of optical counterparts of X-ray binaries.

Visualizing attention in Vision Transformers

by Linn Abraham

AIRIS4D, VOL.4, NO.2, 2026

www.airis4d.com

5.1 Introduction

So far we have been using techniques like Integrated Gradients (IG) for creating saliency maps from a trained (image classification) model. The goal is to give an image for inference and get a prediction but also to be able to visualize how the model came to that prediction and which parts of the image (features, locations in the image) were more important for the prediction. So what we want here is something like a saliency map for a given image - that is, a map which assigns an importance score to each pixel in an image. However, the majority of existing techniques such as IGs were created with CNN models in mind.

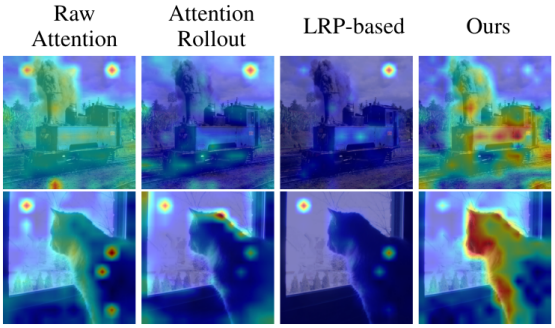

Figure 1: Figure showing the AGCAM heat maps and a comparison with other existing technique taken from the original paper. Method uses two images taken from the PASCAL VOC 2012 for visualizing the self-attention scores.

5.2 Attention-Guided CAM

For transformer-based models like VisionTransformer (ViT), there is a more natural approach of using the attention values learnt by the model to create such saliency maps. Let us look at one such approach called the Attention Guided CAM.

To implement their approach in code lets first try to understand a technique in code called monkey patching.

5.3 Monkey Patching

Monkey patching refers to dynamically modifying or extending code at runtime. The need to do monkey patching arises because of the following. You already have a code base where you have defined your custom ViT architecture which has its custom attention blocks or whatever already defined. The investigation you are doing now is to be done during inference. We do not want to train our model using this modified architecture. But during inference we do want to alter its behaviour. Monkey patching is perfect for this.

The reason why this works in Python is because classes and modules are mutable objects. You can replace a method in a third-party library with your own custom function by simply assigning the new function to the existing attribute name. This can also be quite useful during development when you want to just test things around.

5.4 PyTorch Hooks

The next thing we need to understand is the concept of hooks [1] in PyTorch. A hook is simply a function that you can attach to either a **Tensor** or a **nn.module**

[1] https://www.digitalocean.com/community/tutorials/pytorch-hooks-gradient-clipping-debugging

Patching the Atttention module

```
class PatchedAttention(nn.Module):
    def __init__(self, dim, heads = 8, dim_head = 64, dropout = 0.):
        super().__init__()
        inner_dim = dim_head *  heads
        project_out = not (heads == 1 and dim_head == dim)

        self.heads = heads
        self.scale = dim_head ** -0.5

        self.norm = nn.LayerNorm(dim)

        # hooks for explainability
        self.forward_hook_before_softmax = nn.Identity()
        self.backward_hook_after_softmax = nn.Identity()

        self.attend = nn.Softmax(dim = -1)
        self.dropout = nn.Dropout(dropout)

        self.to_qkv = nn.Linear(dim, inner_dim * 3, bias = False)

        self.to_out = nn.Sequential(
            nn.Linear(inner_dim, dim),
            nn.Dropout(dropout)
        ) if project_out else nn.Identity()
        .
        .
        .
```

Figure 2: Patching the Attention module

Forward function

```
    def forward(self, x):
        x = self.norm(x)
        x = x.detach()

        qkv = self.to_qkv(x).chunk(3, dim = -1)
        q, k, v = map(lambda t: rearrange(t, 'b n (h d) -> b h n d', h = self.heads), qkv)

        dots = torch.matmul(q, k.transpose(-1, -2)) * self.scale

        dots = self.forward_hook_before_softmax(dots)

        attn = self.attend(dots)
        attn = self.dropout(attn)

        attn = self.backward_hook_after_softmax(attn)

        out = torch.matmul(attn, v)
        out = rearrange(out, 'b h n d -> b n (h d)')
        return self.to_out(out)
```

Figure 3: Forward Function

object. This function gets executed automatically when the forward or backward pass happens.

You might encounter hooks in many places — for examples there are hooks that you can attach in a git repository to check your code before a commit gets pushed to the remote etc. Also there are hooks in Linux package managers like ArchLinux's pacman where once a package is installed on your system it runs certain other commands.

In PyTorch hooks are a severely under-documented feature especially considering the functionality that they bring. PyTorch provides two types of hooks:

1. The forward hook — which gets executed during the forward pass
2. The backward hook — which gets executed during the backward pass

5.5 Modify Attention using Hooks

Now lets see all these in action. We first define two hooks as identity layers.

We then modify the forward function as follows. The forward hook gets attached before the softmax function. And the backward hook gets attached after the softmax and the dropout.

Now how do we use this patched attention? Lets look at the following snippet of code. Note that I have only shown the relevant parts of the code. Our custom

Forward function

```
from aarp_ml.torch.model import DeepFlare_ViT
from src.torch.vit.my_agcam import AGCAM

vit_pytorch.vit.Attention = PatchedAttention

model = DeepFlare_ViT(
  height=config.height,
  n_classes=config.n_classes,
  n_passbands=config.n_passbands
).model

model = model.to(device)
model.eval()
ours_method = AGCAM(model)

x, y = next(train_iter)
image = x[0].unsqueeze(0)
image = image.to(device)

with torch.enable_grad():
    # Generate heatmap of our method
    prediction, ours_heatmap = ours_method.generate(image)
```

Figure 4: Using the patched attention to create heatmaps.

ViT model is first imported as usual. Next we monkey patch, i.e., dynamically change the behaviour of the attention block with our PatchedAttention. So that in the next line when our model gets created, it uses our patched version for the attention blocks. Next the rest of the processing happens with the help of the generate function implemented inside the AGCAM class [2]. We import the class first and then we create an object and initialize it by giving it the ViT model we just created that uses the modified attention layers.

Now lets see what happens inside this AGCAM class and the generate function.

Lets zoom in on the loop defined in the constructor function. The for loop iterates over the layers in our model looking for layers which contain the phrase 'before_softmax' and registers Pytorch's forward hook using the get_attn_matrix function. Similarly for layers that contain the phrase 'after_softmax' it attaches the 'full_backward_hook' using the get_grad_attn function.

What do these functions achieve? They simply store the attention matrix values into the empty lists defined in the constructor function.

5.6 Generating heat maps using Attention

Lets put together everything we have learnt so far to understand how the heat maps are generated within the generate function.

- The generate function receives a single input image (batch size of 1).

[2] https://github.com/LeemSaebom/Attention-Guided-CAM-Visual-Explanations-of-Vision-Transformer-Guided-by-Self-Attention

AGCAM class

```python
import torch
from einops.layers.torch import Reduce, Rearrange

class AGCAM:
    """ Implementation of our method."""
    def __init__(self, model, attention_matrix_layer = 'before_softmax', attention_grad_layer = 'after_softmax',
                 head_fusion='sum', layer_fusion='sum'):
        """
        Args:
            model (nn.Module): the Vision Transformer model to be explained
            attention_matrix_layer (str): the name of the layer to set a forward hook to get the self-attention matrices
            attention_grad_layer (str): the name of the layer to set a backward hook to get the gradients
            head_fusion (str): type of head-wise aggregation (default: 'sum')
            layer_fusion (str): type of layer-wise aggregation (default: 'sum')
        """
        self.model = model
        self.head = None
        self.width = None
        self.head_fusion = head_fusion
        self.layer_fusion = layer_fusion
        self.attn_matrix = []
        self.grad_attn = []

        for layer_num, (name, module) in enumerate(self.model.named_modules()):
            if attention_matrix_layer in name:
                module.register_forward_hook(self.get_attn_matrix)
            if attention_grad_layer in name:
                module.register_full_backward_hook(self.get_grad_attn)

    def get_attn_matrix(self, module, input, output):
        # As stated in Methodology part, in ViT with [class] token,
        # only the first row of the attention matrix is directly connected with the MLP head.
        self.attn_matrix.append(output[:, :, 0:1, :]) # shape: [batch, num_heads, 1, num_patches]


    def get_grad_attn(self, module, grad_input, grad_output):
        # As stated in Methodology part, in ViT with [class] token,
        # only the first row of the attention matrix is directly connected with the MLP head.
        self.grad_attn.append(grad_output[0][:, :, 0:1, :]) # shape: [batch, num_heads, 1, num_patches]

    def generate(self, input_tensor, cls_idx=None):
        self.attn_matrix = []
        self.grad_attn = []

        # backpropagate the model from the classification output
        self.model.zero_grad()
        output = self.model(input_tensor)
        _, prediction = torch.max(output, 1)
        self.prediction = prediction
        if cls_idx==None:                               # generate CAM for a certain class label
            loss = output[0, prediction[0]]
        else:                                           # generate CAM for the predicted class
            loss = output[0, cls_idx]
        loss.backward()

        b, h, n, d = self.attn_matrix[0].shape
        self.head=h
        self.width = int((d-1)**0.5)

        # put all matrices from each layer into one tensor
        self.attn_matrix_reverse()
        attn = self.attn_matrix[0]
        gradient = self.grad_attn[0]
        for i in range(1, len(self.attn_matrix)):
            attn = torch.concat((attn, self.attn_matrix[i]), dim=0)
            gradient = torch.concat((gradient, self.grad_attn[i]), dim=0)

        # As stated in Methodology, only positive gradients are used to reflect the positive contributions of each patch.
        # The self-attention score matrices are normalised with sigmoid and combined with the gradients.
        # Here, the variable gradient is the gradients alpha^(k,c)_h in Equation 7 in the methodology part.
        gradient = torch.nn.functional.relu(gradient)
        # Here, the variable attn is the attention score matrices newly normalized with sigmoid,
        # which are equal to the feature maps F^k_h in Equation 2 in the methodology part.
        attn = torch.sigmoid(attn)
        mask = gradient * attn

        # aggregation of CAM of all heads and all layers and reshape the final CAM.
        mask = mask[:, :, 1:].unsqueeze(0)
        mask = Reduce('b l h z p -> b l z p', reduction=self.head_fusion)(mask)
        mask = Reduce('b l z p -> b z p', reduction=self.layer_fusion)(mask)
        mask = Rearrange('b z (h w) -> b z h w', h=self.width, w=self.width)(mask)
```

Figure 5: The AGCAM Class

Registering hooks

```python
    def __init__(self, model, attention_matrix_layer = 'before_softmax', attention_grad_layer = 'after_softmax',
                 head_fusion='sum', layer_fusion='sum'):
        """
        Args:
            model (nn.Module): the Vision Transformer model to be explained
            attention_matrix_layer (str): the name of the layer to set a forward hook to get the self-attention matrices
            attention_grad_layer (str): the name of the layer to set a backward hook to get the gradients
            head_fusion (str): type of head-wise aggregation (default: 'sum')
            layer_fusion (str): type of layer-wise aggregation (default: 'sum')
        """
        self.model = model
        self.head = None
        self.width = None
        self.head_fusion = head_fusion
        self.layer_fusion = layer_fusion
        self.attn_matrix = []
        self.grad_attn = []

        for layer_num, (name, module) in enumerate(self.model.named_modules()):
            if attention_matrix_layer in name:
                module.register_forward_hook(self.get_attn_matrix)
            if attention_grad_layer in name:
                module.register_full_backward_hook(self.get_grad_attn)
```

Figure 6: Registering hooks in the model

Hook functions

```python
    def get_attn_matrix(self, module, input, output):
        # As stated in Methodology part, in ViT with [class] token,
        # only the first row of the attention matrix is directly connected with the MLP head.
        self.attn_matrix.append(output[:, :, 0:1, :]) # shape: [batch, num_heads, 1, num_patches]


    def get_grad_attn(self, module, grad_input, grad_output):
        # As stated in Methodology part, in ViT with [class] token,
        # only the first row of the attention matrix is directly connected with the MLP head.
        self.grad_attn.append(grad_output[0][:, :, 0:1, :]) # shape: [batch, num_heads, 1, num_patches]
```

Figure 7: Defining the hook functions.

- It does a forward pass on the image using the model which (i) uses the patched attention layers and (ii) the PyTorch hooks registered.
- It obtains the predicted class using the max of the predictions.
- It then does a backpropagation step to compute the loss. Now both our hooks would have been triggered and the variables we used to store the attention values and the gradients would have been populated. We then combine the values across the different attention layers using simple summing.
- Next, the self-attention score matrix that we so obtained are normalized using the sigmoid function. It is then multiplied with the gradient matrix to create the final class activation map (CAM).

References

Leem, S., & Seo, H. (2024). *Attention Guided CAM: Visual Explanations of Vision Transformer Guided by Self-Attention*. arXiv preprint arXiv:2402.04563. doi:10.48550/arXiv.2402.04563.

About the Author

Linn Abraham is a researcher in Physics, specializing in A.I. applications to astronomy. He is currently involved in the development of CNN based Computer Vision tools for prediction of solar flares from images of the Sun, morphological classifications of galaxies from optical images surveys and radio galaxy source extraction from radio observations.

Part III

Biosciences

Seed to Callus Revolution: Optimising Germination and Tissue Culture in *Brassica nigra*

by Aengela Grace Jacob

AIRIS4D, VOL.4, NO.2, 2026

www.airis4d.com

1.1 Introduction

Plant Tissue Culture is a technique which involves the aseptic culture of cells, tissue or seed or part of a plant under controlled conditions in vitro. Generally, a part of the tissue usually named as the explant is used to propagate or induce growth. This growth is monitored by providing an essential nutrient medium, adequate temperature, pH and sterile conditions to assist its growth.

Micropropagation(Clonal Propagation) is a technique in which a desired plant material is allowed to regenerate or multiply in vitro under suitable growth conditions. Micropropagation involves four stages:

Stage 0 (selection of desired plant material)

Stage I (establishment of cultures)

Stage II (multiplication of regenerated shoots)

Stage III (rooting of shoots and germination of somatic embryos)

Stage IV (transfer to soil and acclimatization)

Micropropagation is one of the breeding applications of plant tissue culture.

The first commercialization of micropropagation in the 1970s was initiated by Dr Toshio Murashige. The starting material for clonal propagation include parts like node, internode, leaf and buds and root tips. Tissue Culture Techniques involve 4 major steps which discuss the factors to consider during the procedure. These are mainly:

1.Inoculation of Explant

2.Incubation of culture

3.Sub - culturing

4.Transplantation of regenerated plant

1.1.1 Inoculation of Explant

The control of contamination is a crucial step to prevent the entry of microorganisms. Hair,dust are all contaminating agents. A dust free inoculating chamber should be arranged with the person wearing a sterile headgear and clothes inside the culturing area. Preliminary sterilisation should be done inside the chamber and in the hands of the person with 95% alcohol before starting the transferring process.

1.1.2 Incubation of Culture

The cultures after inoculation are incubated at a temperature of around room temperature that is 25 C. In order to prevent contamination of the cultural medium

Some tissues are regenerated well in low light condition (about 1000 lux), regeneration light and dark periods are required, regenerated plantlet well lighted (about 3000 lux) condition and 16h light with 8h dark period is required.

1.1.3 Sub-Culturing

Suspension culture requires the media change or fresh inoculation at short intervals to occur and callus culture requires that the sub-culturing of the callus tissue is done to obtain the callus tissue in dividing conditions.

Depending on the observation made, with the help of hand-lens or upon the help of a simple microscope under aseptic conditions, the explants could have to change to fresh media (newly prepared) or with new components or hormonal formulation in accordance with the condition of cell or tissue growth.

1.1.4 Transplantation of Regenerated Plant

The plants at this time develop adequate root systems and cuticular leaf surface structure so that it can withstand the temperature . Prior to transfer to pots the acclimatization of these regenerated plants are needed. Plants regenerated from in vitro tissue culture are planted in pots in soil.

The medium used to inoculate the explant is the Murashige Skoog medium, it is said to contain a mixture of micro and macronutrients in a balanced form. These nutrients include nitrogen ,phosphorous ,potassium ,calcium (macronutrients) and iron ,copper,manganese

(micronutrients) and various vitamins, solidifying agents like agar and gellan gum and plant growth regulators are added for callus growth.

The seed used as an explant to allow germination and induce callusing was the Brassica nigra (black mustard) which belongs to the brassicaceae family. It is mainly known for its rapid growth and adaptability. It was clearly understood during its germination period that its growth rate was fast. It is said to be a dicot angiosperm belonging to the brassicaceae family. The members of the family of mustard are said to have a cross shape arranged by four petals and has six stamens in which two are short and four are long. The pods of the mustard seed when mature slit open from both sides exposing the seeds. A well known fact says that Egyptian Pharaohs put mustard seeds in their tombs to take with them to the afterlife.

1.1.5 Insights to In vitro Development

Black mustard, *Brassica nigra* is an oil seed, and medicinal cruciferous crop. Developing effective in-vitro germination and tissue-culture systems can enable the acceleration of crop life cycle and preservation of its genetic bases.The most frequent hurdle of plant tissue culture is surface contamination. Black mustard seeds possess a heavy microbial load- bacteria and fungi- on their coats. The protocol followed had the components :70% ethanol (1minute) - 1% sodium hypochlorite (10-15 minutes) - sterile water wash (3 moves) Short, rapid method; has a wide spectrum of considerations. 20 ml mercuric chloride (30 seconds) to sterile water rinse (3x) -Anatoxic; possible seed damage.

The sterility and seed vigor trade-off is observed. Ethanol interferes with the membranes of lipids and renders seeds more susceptible to the bleach, but an excessively long exposure may lead to the process of desiccation. All the procedures seem to be suitable as far as black mustard seeds are concerned. Formation of the callus is characteristic of the totipotency. A 1:6 ratio of cytokinin:auxin is of the essence in Brassica spp.: concentrations of cytokinin stimulate the growth, whereas dedifferentiation is stimulated by auxin. The preparation of Murashige and Skoog (MS) basal medium was with it.

The achievement of germinating in a test tube requires the elimination of mechanical and microbial obstacles and maintenance of seed health. Brief disruption of seed coat lipids by ethanol facilitates increased penetration of the bleach. The Sodium hypochlorite oxidizes surface proteins of the cells, and has the effect of killing bacteria/fungi.

The presence of oxidants in the process destroys the viability of the seeds since they may form reactive oxygen species (ROS) that damage DNA and proteins. Mitigation of this risk is done through rapid rinse protocol (3x sterile water). The tendency to decrease germination in terms of tougher treatments (e.g., mercuric chloride) supports the delicateness of embryonic tissues to the elements of mercury.

The germination of the seed Brassica nigra in the nutrient MS medium was seen around 8-10 days. After

which the seedling was administered for callusing,it was taken under sterile conditions and placed horizontally in the nutrient medium containing the phytohormones BAP and 2,4-D in amounts 0.5mg/L and 3mg/L, it showed callus around 15 th day after inoculation.

1.2 Process Involved

Initially, we make sure the equipment and stock solutions are prepared and are of the accurate concentrations required. The stock concentrations were made in multiples of 10, where Stock A was 10x, Stock B was 1000x, Stock C was 1000x, Stock D was 100x and Stock E was 10x.The seeds of Brassica nigra were collected and washed under running tap water for a minute. The seeds along with the equipment and chemical required for surface sterilization was taken into LAF for sterilisation. The LAf was sterilized using alcohol and UV lights were turned on. 20mL of 2% sodium hypochlorite was added into a 50mL beaker containing the seeds and swirled for about 15 minutes. The hypochlorite solution was discarded and the seeds were washed with distilled water 3-4 times for 2-3 minutes each. 20mL of HgCl2 (0.1%) was poured into the beaker containing seeds and was swirled for about 30 seconds. The metal chloride solution was discarded and the seeds were washed with distilled water 3-4 times for about 2-3 minutes each. Fresh sterile water was added to the beaker containing seeds. This concludes the initial process of surface sterilization of the explant taken.

Further we continue by Inoculation of the explant in which the explant were held using sterile forceps and placed on a sterile filter paper placed in a sterile petri dish. The seeds were dried by rubbing it over the sterile filter paper. The explant was inoculated in the sterile MS media in a sterilised tube.

Finally, the callus formation of the germinated seedling is assessed after 12 days of germination, seedlings were removed from the culture medium under aseptic conditions inside the Laminar Air Flow(LAF).

Explants were taken from different regions of the seedling(Internodes were used as explant) using a sterile scalpel. MS basal medium supplemented with 0.5 mg/L 6-Benzylaminopurine(Cytokinin) and 3.0mg/L 2,4-Dichlorophenoxyacetic acid (2,4-D) (Auxin) was added to the medium. Explants were placed horizontally on the callus induction medium in culture tubes. Cultures were incubated at 25 ± 2°C under complete darkness to promote callus formation.Callus induction was observed over a period of 2 to 3 weeks.

1.3 Results

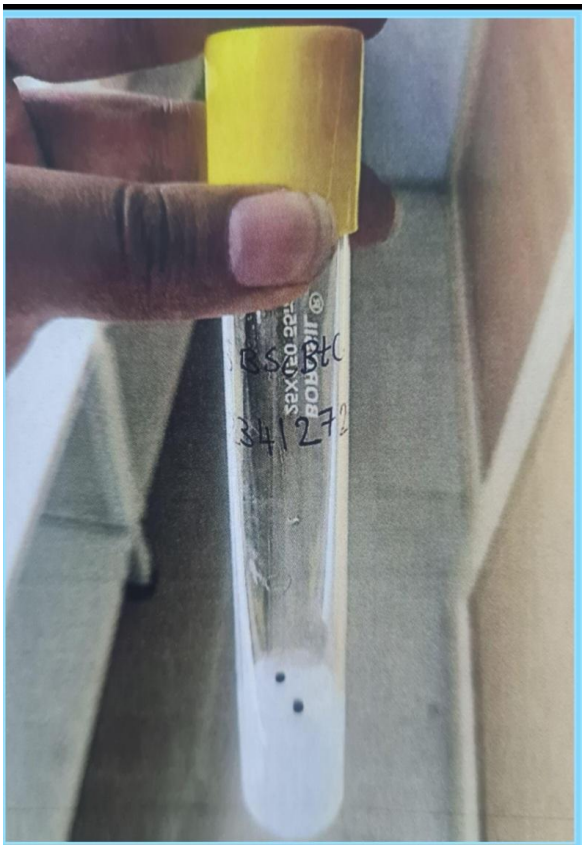

Fig 1. The day of inoculation

As per the given procedure the seeds of *Brassica nigra* were surface sterilised and inoculated in the basal MS medium and incubated at 25 C.

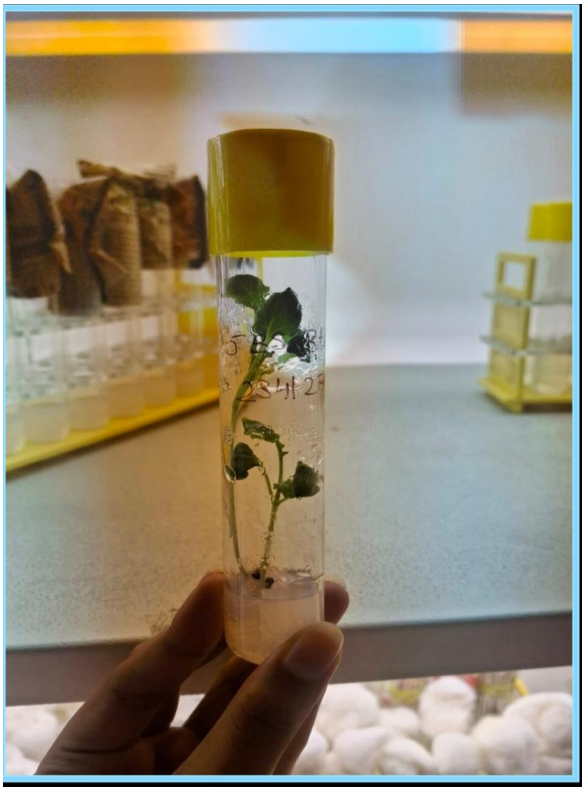

Fig 2: 12th day from inoculation
Germination of the plantlet is seen.

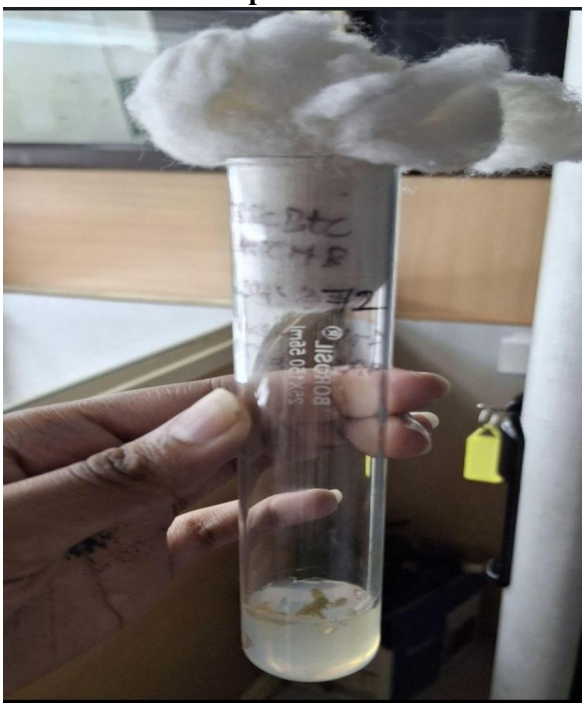

Fig 3 : Callus Induction of *Brassica nigra* (Black mustard)

The inoculated explant (internode) proliferated to form callus on the 15 th day after inoculation of the explant in the nutrient medium.

Fig 4: Callus Induction of the inoculated explant

1.4 Discussion

The project demonstrated the germination of Black Mustard (Brassica nigra) seeds can be reliably achieved through an inoculation protocol carried out within a laminar airflow (LAF) hood, thereby ensuring aseptic conditions throughout the experiment.

By combining effective seed surface-sterilisation, meticulous handling under LAF, and a well-defined callus induction medium, we were able to obtain high rates of germination, promote uniform embryogenic callus formation, and set the stage for downstream tissue-culture applications.

Successful germination began with a two-step sterilisation regimen that proved to be both rapid and thorough. Seeds were first immersed in 70 % ethanol for 30 seconds to disrupt the outer lipid layer, followed immediately by 10 % sodium hypochlorite (NaOCl) solution for 10 minutes. This step was critical for eliminating epiphytic microbes that could otherwise compete with the seedlings or cause contamination.

After the NaOCl treatment, the seeds were rinsed five times with sterile distilled water to remove residual disinfectants. The entire sterilisation process, including rinsing, required roughly 20 minutes per batch, a time that is considerably shorter than more traditional protocols that often extend to 30–45 minutes for NaOCl exposure.

The abbreviated but effective sterilisation schedule not only conserves time but also reduces the risk of chemical damage to the seed coat or embryo. Post-sterilisation, the seeds were placed onto Murashige and Skoog (MS) basal medium supplemented with 3 % (w/v) sucrose and solidified with 0.8 % agar.

The medium was further enriched with a balanced cytokinin–auxin ratio (6-benzylaminopurine 0.5 mg L[207B?]^{1} + 2,4-Dichlorophenoxyacetic acid 3 mg L[207B?]^{1}) to favour callus induction over direct germination. Under controlled photoperiod (16 h light/8 h dark) and temperature (25 ± 2 °C), the sterilised seeds were inoculated directly onto the medium inside the LAF hood, ensuring that no airborne contaminants could interfere with the delicate embryonic tissues. Within 7–10 days, most seeds had germinated, while embryogenic calli were observed emerging from the cotyledonary bases by day 14. The calli displayed a friable, pale green appearance and were indicative of a high totipotent potential, suitable for further sub-culturing or genetic manipulation.

References

Chitralekha Shyam, M. Tripathi, S. Tiwari, and V. Gupta, "In vitro regeneration from callus and cell suspension cultures in Indian mustard [Brassica juncea (Linn.)...," ResearchGate, pp. 1095–1112, May 2021, Accessed: Sep. 10, 2025. [Online].Available:https://www.researchgate.net/publication/351514041_In_vitro_regeneration_from_callus_and_cell_suspension_cultures_in_

M. Ikeuchi, K. Sugimoto, and A. Iwase, "Plant Callus: Mechanisms of Induction and Repression," The Plant Cell, vol. 25, no. 9, pp. 3159–3173, Sep. 2013, doi: https://doi.org/10.1105/tpc.113.116053**.**

"Callus - an overview | ScienceDirect Topics," www.sciencedirect.com. https://www.sciencedirect.com/topics/agricultural-and-biological-sciences/callus

H. Chandran, M. Meena, T. Barupal, and K. Sharma, "Plant tissue culture as a perpetual source for production of industrially important bioactive compounds," Biotechnology Reports, vol. 26, p. e00450, Jun. 2020, doi: https://doi.org/10.1016/j.btre.2020.e00450**.**

"Murashige and Skoog Complete Medium-50X Concentrate liquid | Thermo Fisher Scientific - US," Thermofisher.com, 2025. https://www.thermofisher.com/in/en/home/technical-resources/media-formulation.130.html

A. Varma and A. Jain, "Protocol for Seed Surface Sterilization and In Vitro Cultivation," Biology and Biotechnology of Quinoa, pp. 265–282, 2021, doi: https://doi.org/10.1007/978-981-16-3832-9_13**.**

About the Author

Aengela Grace Jacob is Final Year Student of Bsc Biotechnology , Chemistry (BSc BtC) Dual Major at Christ University Central campus, Bangalore

Gateway to Infection: The Molecular Architecture of Viral Entry into Human T Cells

by Geetha Paul

AIRIS4D, VOL.4, NO.2, 2026

www.airis4d.com

2.1 Introduction

The human immune system relies on the precise coordination of T lymphocytes to identify and eliminate pathogens. The most notable Retroviruses, like HIV-1, have evolved sophisticated mechanisms to bypass the T cell's defence by infiltrating the most secure vault of the cell, the nucleus. This translocation is not a random occurrence but a highly regulated journey through the Nuclear Pore Complex (NPC), a massive proteinaceous gateway embedded in the nuclear envelope. The NPC is composed of approximately 30 different proteins known as Nucleoporins (NUPs), which are organised into a cylindrical structure with eight-fold symmetry. In the context of cell biology and immunology, the interaction between viral proteins and these NUPs represents a critical Protein-Protein Interaction (PPI) that determines whether an infection succeeds or fails.

For a virus to successfully replicate, its genetic material must cross the double-membrane barrier of the nucleus to integrate into the host genome. This process is hindered by the NPC's selective permeability barrier, which naturally excludes molecules larger than 40 kDa. To overcome this, viruses mimic the host's endogenous nuclear transport receptors (karyopherins). The molecular handshake between viral components, such as the viral capsid or Vpr proteins, and specific nucleoporins, like NUP93, NUP188, and the intrinsically disordered FXFG (Phenylalanine-X-Phenylalanine-Glycine) repeats, defines the frontier of modern virology research. Understanding these PPIs is essential for developing entry inhibitors , a class of antiviral drugs designed to lock the nuclear door against viral intruders.

2.2 The Structural Foundation: NUP93 and NUP188

The architectural integrity of the **Nuclear Pore Complex (NPC),** the massive gatekeeper of the cell nucleus, relies heavily on the **Nup93/Nup188 complex**. These proteins are core components of the inner ring, providing the structural scaffolding that supports the transport channel.

2.3 The Role of Nup93: The Adaptor

Nup93 acts as a critical biochemical bridge. It doesn't just sit in the pore; it organises it. Its primary job is to link the inner ring scaffolds to the **channel nucleoporins** (the FG-Nups) that actually filter molecules. **Structure:** Nup93 features a distinctive N-terminal extended helix and a C-terminal ACE1 (Ancestral Coatomer Element 1) domain. **The Velcro Effect:** It uses its N-terminus to tether other proteins, specifically Nup62, Nup58, and Nup54, to the NPC framework. **Stability:** Without Nup93, the inner

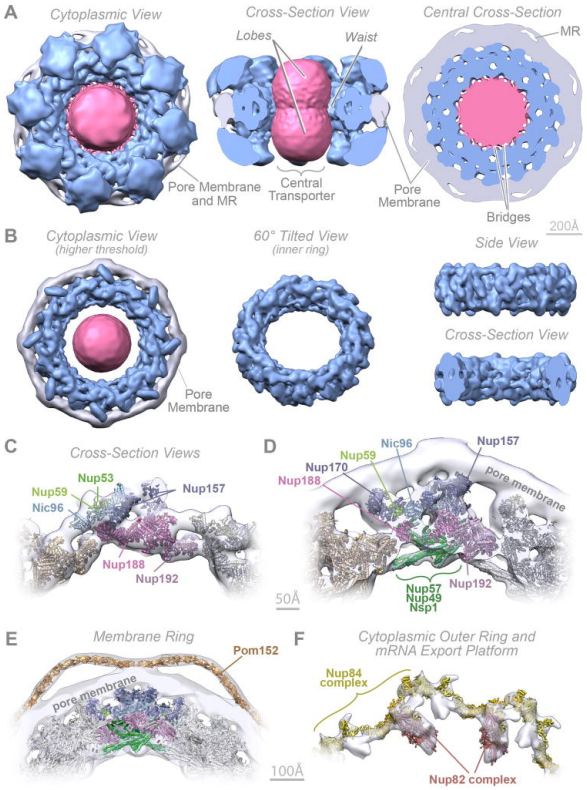

Figure 1: (A–B) Cryo-ET map of the NPC: core scaffold, blue; membrane region, grey; central transporter, pink. MR: membrane ring. (A) (Left) top, cytoplasmic view; (middle) cross-section side view; (right) central cross-section top view. (B) Cryo-ET map is presented at a higher threshold. (Left) top view; (middle) inner ring 60° tilted view; (right) inner ring side (top) and cross-section (bottom) views. Scale bar 200 Å. (C–F) Cross-section views show a representative structure embedded within the Cryo-ET density (grey), presented with different filtering and thresholding, to demonstrate a good fit to the Cryo-ET map in the inner (C, D) and membrane ring (E), the cytoplasmic outer ring, and the mRNA export platform (F). Nups; Scale bar 50 Å (C, D); 100 Å (E, F) Image courtesy: https://pmc.ncbi.nlm.nih.gov/articles/PMC6022767/

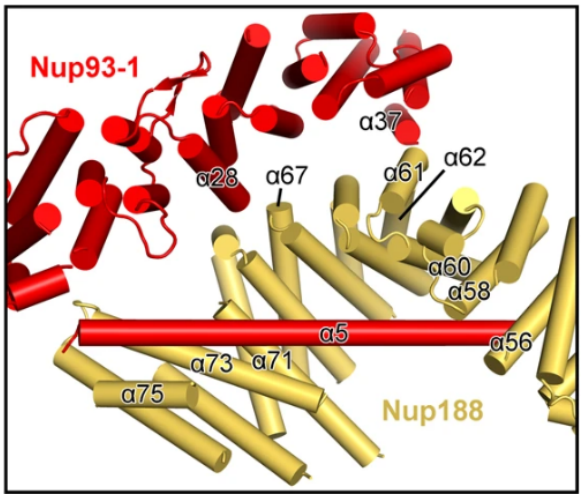

Figure 2: A close-up view on the interface between Nup93-1 and Nup188. Image courtesy: https://www.nature.com/articles/s41422-022-00633-x.pdf

ring loses its connection to the transport machinery, effectively breaking the gate.

2.4 The Role of Nup188: The Large Scaffold

Nup188 is one of the largest proteins in the NPC. Its structure is dominated by **HEAT repeats**, spiral-like motifs that give the protein a flexible, curved, S-shape or C-shape. **Architectural Flexibility:** Because Nup188 is composed of these flexible repeats, it can adjust its conformation to accommodate the massive curvature of the nuclear envelope where the inner and outer membranes fuse. **Functional Redundancy:** Nup188 is often discussed alongside **Nup205**. They are structural paralogs, meaning they share a similar shape and can occupy similar positions within the NPC, though they are not identical in function. **Molecular Sieve:** Recent studies suggest that Nup188 may regulate the passage of integral membrane proteins through the lateral channels of the pore.

At the heart of the NPC's architecture lies the Inner Ring complex, where **NUP93** and **NUP188** serve as the primary structural anchors. In human T cells, NUP93 acts as a linchpin adaptor protein. It possesses a dual-domain functionality: its C-terminus anchors the scaffold to the nuclear membrane, while its N-terminus extends inward to organise the 1 nucleoporin.

From a viral standpoint, NUP93 is a frequent target for subversion. Some viruses utilise proteases to cleave NUP93, effectively dismantling the door frame of the nucleus. This collapse serves a dual purpose: it allows viral components to leak into the nucleus while simultaneously preventing the T cell from exporting messenger RNA (mRNA) encoding antiviral interferons, effectively silencing the cell's alarm system.

NUP188, a paralog of NUP93, provides the necessary flexibility and bolt-like stability to the pore. Its large, S-shaped conformation allows it to act as a structural spacer. In healthy T cells, NUP188 helps regulate the diameter of the central transport channel. During viral entry, certain viral proteins form PPIs with NUP188, inducing conformational shifts in the NPC. By stretching the pore's dimensions, the virus ensures that large pre-integration complexes (PICs), which are often much wider than the pore's standard limit and can pass through without becoming stuck. This structural remodelling is a hallmark of viruses that infect non-dividing or slowly dividing immune cells.

2.5 The Selective Filter: FXFG Peptides and the Hydrophobic Mesh

While NUP93 and NUP188 provide the hardware, the **FXFG peptides** (Phenylalanine-X-Phenylalanine-Glycine repeats) provide the selective software. The selective filter of the nuclear pore complex (NPC) regulates the transport of molecules between the cytoplasm and the nucleus, allowing small molecules to diffuse freely while restricting large molecules unless they are bound to transport receptors. This barrier is formed by the hydrophobic mesh or hydrophobic gel created by phenylalanine-glycine (FG) repeats, specifically FxFG sequences, that fill the NPC central channel. These peptides are found on the disordered tails of nucleoporins that line the interior of the channel. Because Phenylalanine is highly hydrophobic, these tails stick together to form a jelly-like mesh, often described as a beaded curtain.

Viral proteins, specifically the **HIV-1 Capsid (CA)**, have evolved a remarkable ability to navigate this mesh. Through high-resolution crystallography, researchers have identified FG-binding pockets on the surface of the viral capsid.

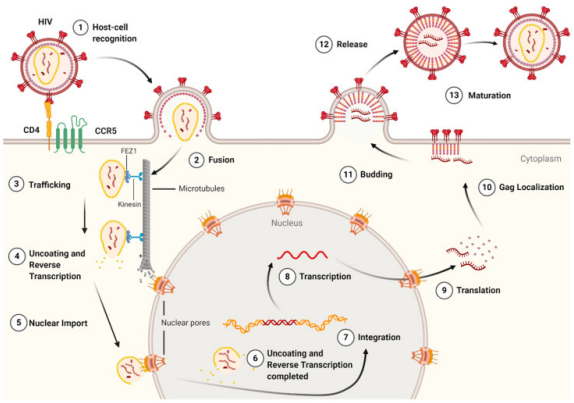

Figure 3: The life cycle of the HIV-1 virus. The early-stage begins with the recognition of host cell receptors (**1**), resulting in the fusion of the virus and release of the viral core into the cytoplasm of the host cell (**2**). This is followed by the trafficking of the core through the cytoplasm (**3**) as reverse transcription and uncoating begins to take place (**4**). Once at the nuclear pore, the viral contents are imported into the nucleus and localized (**5**) to transcriptionally active chromatin while uncoating and reverse transcription are completed (**6**). Following uncoating and reverse transcription, integration occurs (**7**). After the viral genome is integrated into the host cell, viral genes are transcribed (**8**) and translated (**9**) into the Gag polyprotein. The Gag polyprotein then localizes to the host cell membrane (**10**), where budding occurs (**11**), followed by the release of an immature virion (**12**). The final step in the HIV-1 lifecycle is maturation (**13**), where the viral protease cleaves the Gag polyprotein into its constituent, functional proteins. ***Image courtsey:*** https://cdn.ncbi.nlm.nih.gov/pmc/blobs/1a93/7910843/ec34e8ccf0ce/life-11-00100-g003.jpg

The PPI between the viral capsid and the FXFG repeats is transient and low-affinity. This allows the virus to melt through the hydrophobic mesh. The capsid essentially hops from one FXFG peptide to the next, using these repeats as stepping stones to glide into the nucleoplasm. This mimicry is so effective that the T cell's NPC recognises the viral capsid not as a foreign invader, but as a legitimate transport receptor carrying authorised cargo.

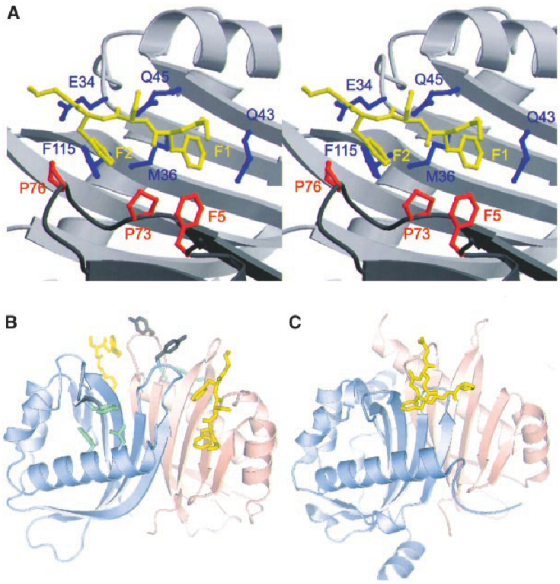

Figure 4: FxFG-repeat cores bind to a hydrophobic depression at the dimer interface of yNTF2. (A) Stereo drawing showing how the FxFG peptide (chain E, yellow) binds to residues from both chains of the NTF2 dimer (chain A, red and chain B, blue). ***Image courtesy:*** https://www.researchgate.net/profile/B-Quimby?_tp=eyJjb250ZXh0Ijp7ImZpcnN0UGFnZSI6Il9kaXJlY3QiLCJwYWdlIjoiX2RpcmVjdCJ9fQ

2.6 Protein-Protein Interactions (PPI) as Therapeutic Targets

The study of PPIs between viral proteins and T cell NUPs has shifted the focus of drug discovery. Traditional antivirals often target viral enzymes (such as reverse transcriptase), but newer Inhibitors of Nuclear Entry target the physical interactions between the virus and its host. By designing small molecules that occupy the FXFG-binding pockets on the viral capsid, scientists can prevent the virus from touching the NUPs. Without this physical contact, the virus remains trapped in the cytoplasm, where it is eventually detected and degraded by the T cell's internal sensors (like cGAS/STING), leading to a successful immune response.

2.7 Protein Interactions in Health and Disease

The precise network of protein-protein interactions is fundamental to maintaining cellular health, and disruptions in this network are at the heart of many diseases. For example, in some cancers, proteins in signalling pathways can become "stuck" in their active, interacting state, leading to uncontrolled cell growth.

An example of a disease caused by abnormal PPIs is Alzheimer's disease. This neurodegenerative condition is characterised by the misfolding and aggregation of proteins in the brain, particularly amyloid-beta and tau. These proteins engage in harmful interactions, forming large, insoluble plaques and tangles that are toxic to neurons and disrupt brain function.

Understanding the role of specific PPIs in disease has opened new avenues for medical treatment. Modern drug development often aims to create molecules that can specifically block a single, disease-causing protein interaction. This targeted approach promises greater precision and potentially fewer side effects. For instance, researchers design small molecules that bind to the interface between two proteins, preventing their interaction and disrupting the disease process.

References

Molecular architecture of the inner ring scaffold of the human nuclear pore complex Science

https://www.science.org/doi/10.1126/science.aaf0643

https://www.researchgate.net/profile/B-Quimby?_tp=eyJjb250ZXh0Ijp7ImZpcnN0UGFnZSI6Il9kaXJlY3QiLCJwYWdlIjoiX2RpcmVjdCJ9fQ

Kim, S. J., et al. (2018). Integrative structure and functional anatomy of a nuclear pore complex. *Nature*, 555(7697), 475-482.

Matreyek, K. A., & Engelman, A. (2013). Viral and cellular determinants of HIV-1 nuclear entry. *Future Virology*, 8(5), 425-442.

Vollmer, B., & Antonin, W. (2014). The control of nuclear pore complex assembly. *Frontiers in Cell and Developmental Biology*, 2, 30.

Lin, J. R., et al. (2020). The Role of NUP93 in Nuclear Transport and Immune Evasion. *Journal of Cell Science*, 133(10).

About the Author

Geetha Paul is one of the directors of airis4D. She leads the Biosciences Division. Her research interests extends from Cell & Molecular Biology to Environmental Sciences, Odonatology, and Aquatic Biology.

Part IV

Computer Programming

Astronomical Computing

by Ajay Vibhute

AIRIS4D, VOL.4, NO.2, 2026

www.airis4d.com

1.1 What Is Astronomical Computing?

1.1.1 Introduction: Why Astronomy Became Computational

Astronomy has always been driven by observation, but over the past century the nature of those observations has changed dramatically. Telescopes have grown larger, detectors more sensitive, and the volume of data generated by modern observatories has reached levels unimaginable in the early 20th century. Where astronomers once analyzed measurements manually, they now rely on sophisticated computational tools to calibrate, reduce, and interpret data. Computational techniques are no longer optional; they have become essential instruments in their own right, enabling discoveries that would be impossible to achieve with human effort alone.

The computational nature of modern astronomy is not limited to number crunching. It encompasses the entire lifecycle of astronomical knowledge: from the initial detection of photons, through data reduction and imaging, to simulations that test theories of cosmic evolution. In this sense, astronomical computing forms the backbone of the field, linking hardware, software, and human insight in the quest to understand the universe.

1.1.2 Historical Roots of Astronomical Computing

The roots of astronomical computing trace back to the era of celestial navigation and the manual calculation of ephemerides, tables predicting the positions of planets, moons, and stars. Before digital computers, astronomers relied on logarithmic tables, mechanical calculators, and punched cards to perform these complex calculations. Tasks that could take weeks or months required careful, repetitive human effort, often carried out by dedicated observatory staff. The mid-20th century brought a revolution with the arrival of digital computers. Mainframes such as the IBM 704 enabled astronomers to automate calculations for stellar motions, orbital mechanics, and the reduction of photographic plates. This computational power made large-scale projects feasible, including the Hipparcos satellite, which precisely measured the positions of over 100,000 stars, and the Sloan Digital Sky Survey (SDSS), which mapped

Figure 1: Modern observatories generate vast amounts of data requiring computational analysis.

millions of celestial objects across multiple wavelengths. These initiatives demonstrated that computation could turn raw measurements into quantitative, statistically robust insights, enabling discoveries that would have been impossible by hand. By the late 20th century, the concept of a computational pipeline became standard. Pipelines automate the conversion of raw measurements into scientifically meaningful data products, typically including calibration, noise reduction, and integration of multiple observations. Modular pipelines allow algorithms to be adjusted or replaced without reprocessing entire datasets, enhancing efficiency, reproducibility, and transparency. The historical progression shows a clear trend: as astronomical data volumes increased, so did the need for robust computational methods. What began as manual calculation has evolved into sophisticated software systems capable of processing terabytes of data, integrating multiple instruments, and performing complex analyses. Today, computational methods are an inseparable part of astronomical observation, acting both as a tool for measurement and a lens through which the cosmos is interpreted.

Figure 2: Early computational tools such as punch cards and mainframes were pivotal in large-scale astronomical calculations.

1.1.3 What Makes Astronomical Data Different

Astronomical data differ from typical datasets in several fundamental ways. Observations are inherently constrained by the physical properties of detectors, including sensitivity, dynamic range, and pixel scale, as well as by the environment—for ground-based telescopes, atmospheric turbulence blurs images, introduces background light, and limits faint-source detection. Even in space-based observatories, limitations such as cosmic ray hits, thermal noise, and finite detector resolution affect the raw measurements. Noise is unavoidable and arises from multiple sources: photon statistics, electronic readout fluctuations, cosmic ray events, and background contamination. Each measurement is also convolved with the instrument's response function—for instance, the point-spread function (PSF) in imaging or the spectral response in spectrographs—meaning that raw counts are only an indirect representation of the intrinsic physical quantities astronomers wish to measure. Astronomical datasets are also massive and multi-dimensional. Large surveys can catalog billions of objects, each with repeated measurements over time, across multiple wavelengths, and sometimes in different polarization states. The data are structured in intertwined spatial, temporal, and spectral dimensions, forming a complex, high-dimensional space. This richness enables deep scientific insights but also requires sophisticated computational methods for analysis, such as image deconvolution, time-series modeling, and multi-wavelength cross-correlation. These unique challenges distinguish astronomical computing from conventional data science, emphasizing the need for specialized algorithms, carefully designed pipelines, and domain-specific data management techniques capable of handling scale, complexity, and uncertainty inherent to the cosmos.

1.1.4 Computing as an Astronomical Instrument

Computation in astronomy is not merely a tool for processing data; it functions as a scientific instrument in its own right. Just as a spectrograph disperses light to reveal the chemical composition of a star, or a radio dish converts incoming waves into measurable voltages, computational algorithms transform raw measurements into scientifically meaningful information. Algorithms such as image deconvolution, interpolation, source extraction, and statistical modeling do more than

automate analysis—they actively shape the data, determining which structures, correlations, or subtle signals can be recovered from noisy observations. The choice of method, the parameters selected, and the assumptions embedded in the algorithm all influence the final scientific result, much like the optical design and calibration of a physical instrument. Modern astronomical software often integrates simulation, forward modeling, and visualization tools, allowing researchers to explore not only what the data show but also how uncertainties propagate through analysis pipelines. For example, synthetic images can be generated with known noise and instrumental effects to test the fidelity of deconvolution algorithms, while Monte Carlo simulations can assess the reliability of derived parameters such as stellar mass or distance. By enabling these tests and providing interpretive frameworks, computation extends the capabilities of telescopes, allowing astronomers to make discoveries that would be impossible through hardware alone. In effect, software pipelines, models, and computational methods collectively act as virtual instruments, complementing and amplifying the power of physical observatories.

1.1.5 Scope and Boundaries of the Field

Astronomical computing encompasses a broad and diverse range of activities that touch nearly every stage of modern observational and theoretical astronomy. It begins with data acquisition and calibration, ensuring that raw signals from telescopes are accurately recorded and corrected for instrumental and environmental effects. From there, it extends to data reduction and analysis, where algorithms transform noisy, incomplete, or high-dimensional measurements into scientifically meaningful quantities. Beyond observation, astronomical computing also includes the simulation of astrophysical phenomena, from galaxy formation to stellar evolution, allowing researchers to compare theoretical predictions with observations. To make sense of these massive and complex datasets, scientists employ advanced visualization techniques, exploring multi-dimensional parameter spaces and temporal sequences that would be impossible to interpret manually. Finally, the field requires robust data management and archiving systems capable of handling petabyte-scale datasets and ensuring long-term accessibility for both current and future research. Despite this breadth, astronomical computing is constrained by the physical limitations of instruments, the stochastic nature of photons, and the computational resources available. Large datasets and high-resolution simulations push the boundaries of storage, memory, and processing power, necessitating careful design of algorithms and pipelines to achieve both efficiency and accuracy. Recognizing these limitations is critical for building robust analysis frameworks and correctly interpreting the results. Astronomical computing is inherently interdisciplinary, drawing upon principles from computer science, statistics, applied mathematics, and physics, while being tightly coupled to the practical and scientific needs of astronomy. Researchers must strike a delicate balance between algorithmic sophistication, computational feasibility, and physical fidelity. Sophisticated methods are only valuable if they produce results that are interpretable, reproducible, and scientifically meaningful, bridging the gap between raw data and our understanding of the cosmos.

1.1.6 Summary and Outlook

Astronomical computing represents the intersection of observation, theory, and computation. It transforms vast, noisy, and complex datasets into structured knowledge about the universe. The field has grown from simple calculations to sophisticated pipelines and simulations, forming a central component of modern astronomy. Looking ahead, continued increases in data volume and complexity will further integrate computation into every stage of astronomical research, making the development of robust, transparent, and efficient computational methods more crucial than ever.

About the Author

Dr. Ajay Vibhute is currently working at the National Radio Astronomy Observatory in the USA. His research interests mainly involve astronomical imaging techniques, transient detection, machine learning, and computing using heterogeneous, accelerated computer architectures.

The Disappearing Role of Judgment in Automated Systems

by Jinsu Ann Mathew

AIRIS4D, VOL.4, NO.2, 2026

www.airis4d.com

Automation doesn't usually arrive as a bold decision. It slips in quietly.

A recommendation replaces a choice. A score replaces a conversation. A system that once suggested now decides. Over time, no one remembers exactly when judgment stopped being exercised and started being assumed.

In many modern systems, humans are still present, but mostly as spectators. Algorithms produce rankings, flags, or predictions, and these outputs move smoothly into action. The human role is often limited to approving what the system already decided — or stepping in only when something goes visibly wrong.

What disappears in this process is not control, but judgment. Judgment is the ability to pause, question, and interpret. It is the capacity to say "this may be correct, but it doesn't fit this situation." When systems are designed to minimize friction, that pause becomes inconvenient, and disagreement starts to feel like an error.

This article explores how judgment is quietly designed out of automated systems, why that happens, and what we risk losing when decisions become efficient but unexamined.

2.1 Prediction Quietly Becomes Decision

Consider this example. A large company introduces an automated system to help screen job applications. The goal is not to replace human recruiters, but to manage volume. The system scores resumes and ranks candidates so recruiters can focus their attention more efficiently.

In the beginning, recruiters use the ranking as a guide. They scroll through the list, occasionally opening lower-ranked profiles out of curiosity. The system feels like a helpful assistant.

Over time, the workflow changes. Only the top-ranked candidates are reviewed. Others are rarely seen. There is no rule forbidding recruiters from checking the rest, but doing so feels unnecessary and time-consuming. Trust in the system grows, not because it is perfect, but because it is consistent.

Eventually, the ranking stops being a suggestion and starts functioning as a decision. Candidates filtered out by the system effectively disappear from consideration, even though a human is still officially "in charge."

This is how prediction quietly becomes decision. Authority is not transferred through policy or instruction, but through habit. When a system is always present, always confident, and rarely questioned, its outputs begin to define the boundaries of action.

The human role remains, but it changes in nature. Judgment is no longer exercised across all cases. It is reserved only for those situations where the system clearly fails. Most decisions happen automatically, without anyone explicitly deciding that they should.

What is lost is not oversight, but engagement. When predictions are treated as conclusions, judgment

fades — not because it is forbidden, but because it is no longer required.

2.2 Automation Bias, Objectivity, and the Loss of Responsibility

Once automated systems become routine, trust in them stops being an active choice and becomes a default. Outputs arrive as scores, rankings, or flags, and these formats carry an air of objectivity. They look neutral, precise, and detached from human judgment.

This appearance matters. Disagreeing with a system requires effort and explanation, while agreeing requires none. Over time, this imbalance shapes behavior. People do not blindly follow machines; they follow them because it is easier, safer, and institutionally encouraged.

As trust shifts, responsibility begins to blur. Decisions feel justified by process rather than owned by individuals. When outcomes are questioned, the answer often points elsewhere: the model, the threshold, the workflow. Each step is defensible on its own, yet the decision as a whole has no clear owner.

This is not a failure of intention. It is a structural consequence of systems designed to minimize friction. Efficiency removes pauses. Consistency removes discretion. What disappears along the way is the moment where someone must say, this decision is mine.

The result is a peculiar kind of authority without accountability. Automated decisions feel final, yet responsibility is diffused across designers, operators, and policies. When things work, this diffusion goes unnoticed. When they fail, it becomes a serious problem.

2.3 Judgment as a Skill That Fades

Judgment is not a switch that can be turned on when needed. It is a skill maintained through regular use. When automated systems handle most decisions, humans lose opportunities to practice interpreting context, weighing exceptions, and noticing subtle signals.

Over time, this changes the human role. People become monitors rather than decision-makers. They learn how to manage systems, not how to judge situations. When rare or unfamiliar cases appear, intervention becomes difficult precisely because judgment has not been exercised regularly.

This creates a fragile dependency. Systems work smoothly under familiar conditions, but when reality drifts outside their assumptions, the humans overseeing them are least prepared to step in. Failures appear sudden, even though the conditions for failure have been building quietly.

In this sense, automation does not merely remove judgment from daily decisions — it erodes the capacity for judgment itself.

2.4 Stability Hides Fragility

Consider an automated navigation system used by emergency response teams to determine the fastest route to an incident. Under normal conditions, the system works exceptionally well. It accounts for traffic, distance, and historical patterns, and responders learn to trust it without hesitation.

During a large public event, however, conditions change. Roads are closed unexpectedly, temporary barriers appear, and crowd movement alters traffic in ways the system has not seen before. The navigation system continues to recommend routes that are technically optimal but practically unusable.

Responders hesitate. Deviating from the system feels risky, especially under pressure. Following it feels defensible. Minutes are lost before someone decides to rely on local knowledge rather than the automated guidance.

The failure appears sudden, but it is not accidental. The system was designed for efficiency in stable conditions, not for judgment under uncertainty. Over time, responders had stopped actively reasoning about routes because the system rarely required them to do so.

This is how stability hides fragility. When automation works well most of the time, it discourages

independent judgment. When conditions change, the system's confidence becomes a liability, and human intervention arrives too late.

What looks like a routing error is, at its core, a judgment failure that developed long before the crisis.

2.5 Reintroducing Judgment by Design

If judgment disappears because systems make decisions too easily, then bringing it back requires deliberate design choices.

Consider an automated loan approval system used by a bank. For most applications, the system works smoothly. Applicants are approved or rejected within seconds, and human officers are rarely involved. The process is fast, consistent, and efficient.

Now imagine an applicant with an unusual profile — a freelancer with irregular income but a long history of timely repayments. The system rejects the application because it does not fit familiar patterns. A human officer can technically override the decision, but doing so requires extra documentation, justification, and approval. Following the system is easier.

Over time, officers stop intervening. Not because they disagree less, but because the system makes disagreement inconvenient.

Designing for judgment means avoiding this situation. If humans are expected to exercise judgment, systems must make it practical to do so. Questioning a decision should not feel like breaking the process. Overrides should be part of normal operation, not treated as exceptions.

Judgment also needs practice. If humans only step in during rare failures, they lose confidence and context. Systems should encourage regular review and engagement, even when everything appears to be working. This keeps people familiar with how decisions are made and where their limits lie.

Reintroducing judgment does not mean rejecting automation. It means using automation to handle routine cases while preserving human responsibility for interpretation, edge cases, and consequences. When judgment is designed into the system, automation becomes more reliable — not less.

2.6 Conclusion - Keeping Judgment in the Loop

Automated systems have become part of everyday decision-making, often without much notice. They help us move faster, process more information, and maintain consistency at scale. Used well, they are powerful tools.

Problems arise when efficiency quietly replaces judgment. When decisions flow smoothly from prediction to action, the human role shrinks — not because people are excluded, but because they are no longer needed to think. Responsibility becomes diffused, intervention becomes rare, and failures feel sudden when they occur.

Judgment is not an obstacle to good systems. It is what allows systems to adapt when conditions change, rules break down, or consequences matter more than speed. Removing judgment may make systems efficient, but it also makes them fragile.

The question, then, is not how much automation we should adopt, but how we design it. Systems should handle repetition and scale, while leaving room for human interpretation, disagreement, and responsibility. When judgment remains part of the process, automation does not replace human decision-making — it strengthens it.

In the end, the most reliable systems are not those that eliminate judgment, but those that know where it still belongs.

References

- IRONIES OF AUTOMATION
- Humans and Automation: Use, Misuse, Disuse, Abuse
- Concrete Problems in AI Safety
- Thinking, Fast and Slow.

About the Author

Jinsu Ann Mathew is a research scholar in Natural Language Processing and Chemical Informatics. Her interests include applying basic scientific research on computational linguistics, practical applications of human language technology, and interdisciplinary work in computational physics.

About airis4D

Artificial Intelligence Research and Intelligent Systems (airis4D) is an AI and Bio-sciences Research Centre. The Centre aims to create new knowledge in the field of Space Science, Astronomy, Robotics, Agri Science, Industry, and Biodiversity to bring Progress and Plenitude to the People and the Planet.

Vision

Humanity is in the 4th Industrial Revolution era, which operates on a cyber-physical production system. Cutting-edge research and development in science and technology to create new knowledge and skills become the key to the new world economy. Most of the resources for this goal can be harnessed by integrating biological systems with intelligent computing systems offered by AI. The future survival of humans, animals, and the ecosystem depends on how efficiently the realities and resources are responsibly used for abundance and wellness. Artificial intelligence Research and Intelligent Systems pursue this vision and look for the best actions that ensure an abundant environment and ecosystem for the planet and the people.

Mission Statement

The 4D in airis4D represents the mission to Dream, Design, Develop, and Deploy Knowledge with the fire of commitment and dedication towards humanity and the ecosystem.

Dream

To promote the unlimited human potential to dream the impossible.

Design

To nurture the human capacity to articulate a dream and logically realise it.

Develop

To assist the talents to materialise a design into a product, a service, a knowledge that benefits the community and the planet.

Deploy

To realise and educate humanity that a knowledge that is not deployed makes no difference by its absence.

Campus

Situated in a lush green village campus in Thelliyoor, Kerala, India, airis4D was established under the auspicious of SEED Foundation (Susthiratha, Environment, Education Development Foundation) a not-for-profit company for promoting Education, Research. Engineering, Biology, Development, etc.

The whole campus is powered by Solar power and has a rain harvesting facility to provide sufficient water supply for up to three months of drought. The computing facility in the campus is accessible from anywhere through a dedicated optical fibre internet connectivity 24×7.

There is a freshwater stream that originates from the nearby hills and flows through the middle of the campus. The campus is a noted habitat for the biodiversity of tropical Fauna and Flora. airis4D carry out periodic and systematic water quality and species diversity surveys in the region to ensure its richness. It is our pride that the site has consistently been environment-friendly and rich in biodiversity. airis4D is also growing fruit plants that can feed birds and provide water bodies to survive the drought.